Resource

Cell Stem Cell

Prospective Isolation of Poised iPSC Intermediates Reveals Principles of Cellular Reprogramming

Graphical Abstract

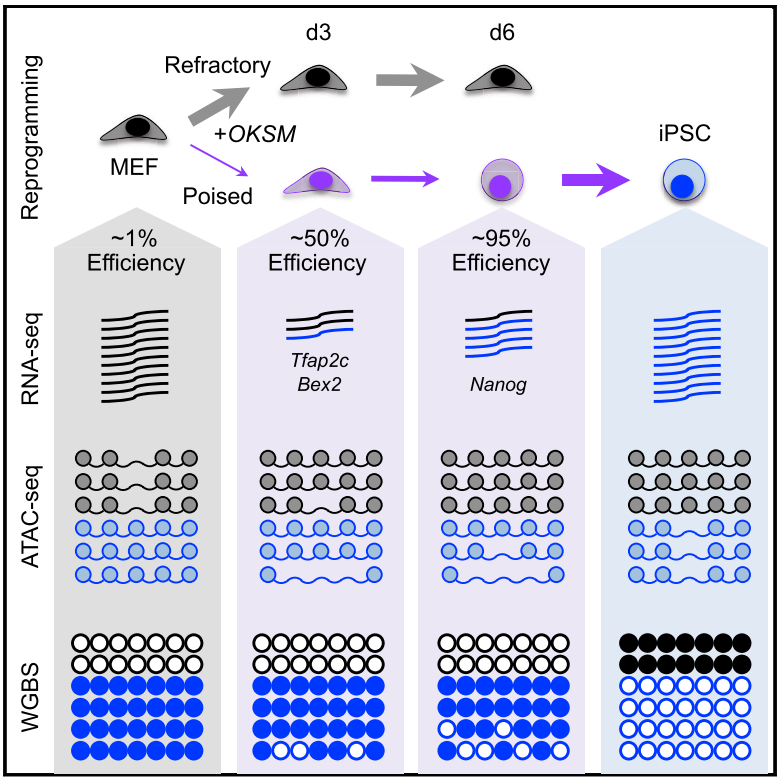

Authors

Benjamin A. Schwarz, Murat Cetinbas, Kendell Clement, ..., Alexander Meissner, Ruslan I. Sadreyev, Konrad Hochedlinger

Correspondence

hochedlinger@molbio.mgh.harvard.edu

In Brief

Cellular reprogramming to induced pluripotent stem cells (iPSCs) is typically inefficient, complicating mechanistic analyses. Schwarz et al. use cell surface marker combinations to identify and molecularly characterize early intermediates poised to reprogram with up to 95% efficiency.

Highlights

- Cell surface markers allow isolation of rare intermediates poised to reprogram
- Transcriptional analysis of poised cells uncovers early regulators of reprogramming
- Chromatin accessibility changes rapidly in reprogramming and precedes transcription
- An early wave of DNA demethylation occurs in poised reprogramming intermediates

Schwarz et al., 2018, Cell Stem Cell *23*, 289–305
August 2, 2018
https://doi.org/10.1016/j.stem.2018.06.013

CellPress

Cell Stem Cell
Resource

Prospective Isolation of Poised iPSC Intermediates Reveals Principles of Cellular Reprogramming

Benjamin A. Schwarz,[1,2,3,4] Murat Cetinbas,[1,5] Kendell Clement,[3,6] Ryan M. Walsh,[1,2,3] Sihem Cheloufi,[1,2,3] Hongcang Gu,[6] Jan Langkabel,[7] Akihide Kamiya,[8] Hubert Schorle,[7] Alexander Meissner,[2,3,6,9] Ruslan I. Sadreyev,[1,4] and Konrad Hochedlinger[1,2,3,10,*]

[1]Department of Molecular Biology, Cancer Center, and Center for Regenerative Medicine, Massachusetts General Hospital, 185 Cambridge Street, Boston, MA 02114, USA
[2]Harvard Stem Cell Institute, 1350 Massachusetts Avenue, Cambridge, MA 02138, USA
[3]Department of Stem Cell and Regenerative Biology, Harvard University, Cambridge, MA 02138, USA
[4]Department of Pathology, Massachusetts General Hospital, 55 Fruit Street, Boston, MA 02114, USA
[5]Department of Genetics, Harvard Medical School, Boston, MA 02115, USA
[6]Broad Institute of MIT and Harvard, Cambridge, MA 02142, USA
[7]University of Bonn Medical School, Institute of Pathology, Department of Developmental Pathology, Bonn, Germany
[8]Department of Molecular Life Sciences, Tokai University School of Medicine, 143 Shimokasuya, Isehara, Kanagawa, Japan
[9]Present address: Max Planck Institute for Molecular Genetics, 14195 Berlin, Germany
[10]Lead Contact
*Correspondence: hochedlinger@molbio.mgh.harvard.edu
https://doi.org/10.1016/j.stem.2018.06.013

SUMMARY

Cellular reprogramming converts differentiated cells into induced pluripotent stem cells (iPSCs). However, this process is typically very inefficient, complicating mechanistic studies. We identified and molecularly characterized rare, early intermediates poised to reprogram with up to 95% efficiency, without perturbing additional genes or pathways, during iPSC generation from mouse embryonic fibroblasts. Analysis of these cells uncovered transcription factors (e.g., *Tfap2c* and *Bex2*) that are important for reprogramming but dispensable for pluripotency maintenance. Additionally, we observed striking patterns of chromatin hyperaccessibility at pluripotency loci, which preceded gene expression in poised intermediates. Finally, inspection of these hyperaccessible regions revealed an early wave of DNA demethylation that is uncoupled from *de novo* methylation of somatic regions late in reprogramming. Our study underscores the importance of investigating rare intermediates poised to produce iPSCs, provides insights into reprogramming mechanisms, and offers a valuable resource for the dissection of transcriptional and epigenetic dynamics intrinsic to cell fate change.

INTRODUCTION

Cellular reprogramming refers to the process by which differentiated somatic cells are converted into induced pluripotent stem cells (iPSCs) upon ectopic expression of defined transcription factor (TF) combinations, typically *Oct4* (*Pou5f1*), *Klf4*, *Sox2*, and *Myc* (*OKSM*) (Takahashi and Yamanaka, 2006). This technology has enormous potential for regenerative medicine, disease modeling, and drug screening as well as the study of cell fate change following forced redirection of cellular identity (Takahashi and Yamanaka, 2016). However, reprogramming is generally slow (>2 weeks) and inefficient (<1%), complicating mechanistic studies. Most cells fail to reprogram, indicating the existence of epigenetic barriers as well as the requirement for additional facilitators of this process, which remain largely unidentified. Because cells that do not contribute to successful reprogramming dominate assays that rely on bulk reprogramming cultures, it is imperative to identify and examine those select cells poised to generate iPSCs to gain insights into the underlying mechanisms.

Our laboratory and others previously characterized intermediate stages of reprogramming from mouse embryonic fibroblasts (MEFs) to iPSCs using surface markers (Brambrink et al., 2008; Polo et al., 2012; Stadtfeld et al., 2008). Briefly, we have shown that Thy1 is expressed by MEFs and intermediates that are refractory to reprogramming but lost by early intermediates with iPSC potential. A subset of Thy1$^-$ intermediates then upregulates SSEA-1 before activating an *Oct4*-GFP reporter at later time points, which coincides with the acquisition of a stable, transgene-independent pluripotent state. Although SSEA-1 expression significantly enriches for intermediates that successfully progress toward iPSCs, this population remains heterogeneous and inefficient in conventional reprogramming assays (5%–10% reprogramming efficiency).

Recently, the utility of SSEA-1 as a prospective reprogramming marker has been challenged, and other marker combinations, such as CD44 and ICAM1 (O'Malley et al., 2013) or CD49d and CD73 (Lujan et al., 2015), have been proposed. However, the relevance of ICAM1 has only been demonstrated at a late time point using a highly efficient reprogramming system, whereas CD49d and CD73 were exclusively tested at early

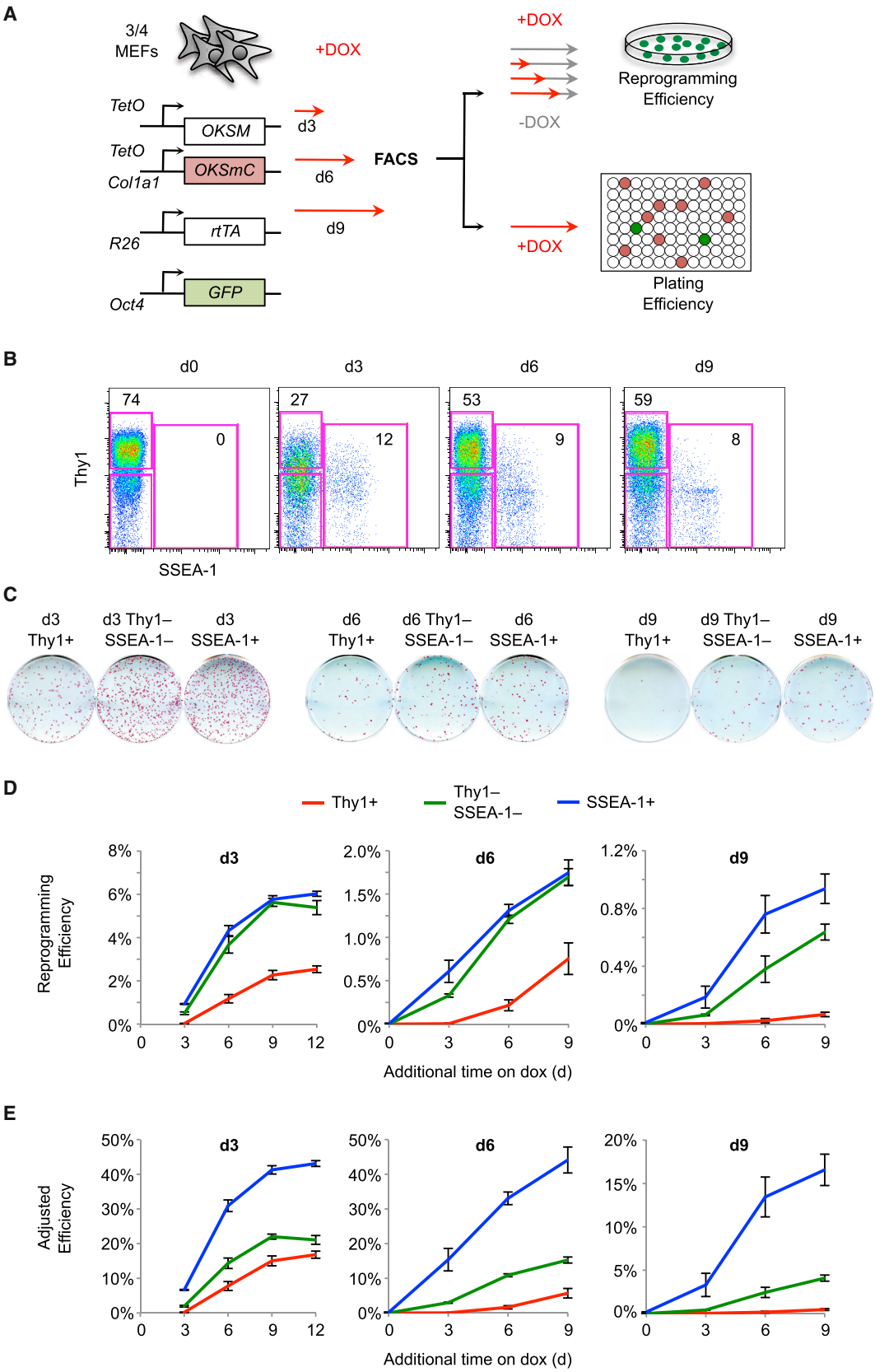

(legend on next page)

stages of reprogramming using an inefficient and heterogeneous retroviral reprogramming system. Thus, there is no current consensus on which markers are the most useful for isolating cells poised to produce iPSCs. Additionally, no previously reported enrichment protocol has achieved reprogramming efficiencies of greater than 10%–15% for early intermediates (Lujan et al., 2015; Polo et al., 2012). To resolve these discrepancies, it will be critical to compare published markers and identify additional markers using the same reprogramming conditions. Furthermore, it will be important to account for the differential ability of sorted cells to survive and adhere to cell culture plates (plating efficiency) because this could profoundly skew the measure of reprogramming efficiency.

Here we validate that SSEA-1 is an early predictive marker of reprogramming progression when adjusting for plating efficiency. By systematically testing over a dozen additional markers, we found that Sca-1 and either CD73 (on day 3) or epithelial cell adhesion molecule (EpCAM) (on day 6) subdivide the SSEA-1$^+$ population and allow for the enrichment of early intermediates poised to produce iPSCs with unparalleled efficiencies of up to 95%. We finally exploit this approach to define the dynamics of transcription, chromatin accessibility, and DNA methylation patterns in those rare cells poised to produce iPSCs, revealing unexpected principles about the process of TF-induced cell fate change.

RESULTS

Plating Efficiency Profoundly Affects Measures of Reprogramming Potential

"Three/four" (3/4) MEFs were derived from mice heterozygous for *Col1a1-tetO-OKSM*, a tetracycline-inducible polycistronic 4-factor vector; *Col1a1-tetO-OKSmCherry*, a tetracycline-inducible polycistronic 3-factor vector with a fluorescent reporter; *Rosa26-M2rtTA*; and an *Oct4-GFP* knockin allele (Figure 1A; Bar-Nur et al., 2014; Stadtfeld et al., 2010). This system ensures near-homogeneous *OKSM* expression, is highly reproducible, and allows for temporal control of reprogramming by adding or removing doxycycline (dox). Furthermore, the *mCherry* allele allows us to track expression of the *Oct4*, *Klf4*, *Sox2* (*OKS*) transgene and to differentiate mCherry$^+$ reprogramming cells from mCherry$^-$ feeders. Unless otherwise specified, all reprogramming assays were performed in the presence of 15% serum, 1,000 U/mL leukemia inhibitory factor (LIF), and 50 μg/mL ascorbic acid (AA).

Following dox exposure, a subset of 3/4 MEFs rapidly loses Thy1 and gains SSEA-1 expression (Figure 1B). To determine the functional significance of these markers, we employed fluorescence-activated cell sorting (FACS) to isolate Thy1$^+$, Thy1$^-$SSEA-1$^-$, and SSEA-1$^+$ intermediates. Sorted cells were then re-plated on feeders and allowed to continue reprogramming for additional days on dox. After a period of dox withdrawal, the numbers of iPSC colonies were determined by alkaline phosphatase (AP) staining to calculate reprogramming efficiencies (Figure 1A, top). We confirmed that all dox-independent AP$^+$ colonies were *Oct4*-GFP$^+$ (Figure S1A) and have previously demonstrated that AP$^+$ colonies obtained with this system are Nanog$^+$ and support the development of germline chimeras (Bar-Nur et al., 2014), indicating that they represent *bona fide* iPSCs. Consistent with our prior results (Polo et al., 2012; Stadtfeld et al., 2008), Thy1$^+$ cells had poor reprogramming potential at every time point, and their ability to form iPSCs progressively decreased during the reprogramming time course (Figures 1C and 1D). However, contrary to our previous findings, SSEA-1$^+$ cells were no better than Thy1$^-$SSEA-1$^-$ intermediates until late in reprogramming.

To measure reprogramming efficiencies, we have to disrupt the reprogramming process by dissociating plate-adherent cells, exposing them to the high pressures of cell sorting, and then re-plate them. Few cells survive this process, which could explain our low measure of reprogramming efficiency. Furthermore, if different intermediates exhibit differential survival rates, then this could greatly bias our results. To account for these important variables, we devised a plating efficiency assay. Briefly, defined numbers of cells were sorted onto feeders in 96-well plates, and the limiting dilution (LD) of cells required to detect mCherry$^+$ and/or *Oct4*-GFP$^+$ progeny was determined for each intermediate population (Figures S1B–S1F). We chose LD over a single cell assay because LD is more robust, allowing us to more precisely assess a wider range of possible plating efficiencies using fewer plates. Nevertheless, we confirmed that plating efficiencies calculated by LD were equivalent to those determined by sorting single cells for day 3 intermediates (Figure S1G). 10,000 cells from the same sort were also transferred to 6-well plates to determine reprogramming efficiencies (Figure 1A). Adjusted reprogramming efficiencies were calculated by dividing reprogramming efficiencies by plating efficiencies for each sorted population. Correcting for plating efficiency improved the overall efficiency of live cells from ~1% to ~7% on day 3 and from ~1% to ~12% on day 6 of *OKSM* induction (Figure S1H). Critically, by accounting for plating efficiency, SSEA-1 emerges as an important marker of reprogramming progression at every examined time point (Figure 1E), confirming previous observations by our group. Furthermore, studies that concluded that SSEA-1 was not an early predictive marker of reprogramming did not assess differential plating (Lujan et al., 2015; O'Malley et al., 2013). Finally, the actual reprogramming potential of SSEA-1$^+$ cells is remarkably high (~40% on day 3

Figure 1. SSEA-1 Identifies Progressing Reprogramming Intermediates

(A) Experimental scheme.

(B) Flow analysis of 3/4 MEF reprogramming. Shown are representative plots with the percentage of cells in the Thy1$^+$ and SSEA-1$^+$ gates.

(C) Reprogramming efficiency of Thy1$^+$, Thy1$^-$SSEA-1$^-$, and SSEA-1$^+$ populations. Shown are representative AP stains of wells exposed to dox for 9 additional days, followed by a period of dox withdrawal.

(D) Reprogramming efficiency was calculated by dividing the number of AP$^+$ dox-independent iPSC colonies by the number of cells plated for each of the indicated time points. Results are shown as the mean of 3 experiments ± 1 SD.

(E) Adjusted reprogramming efficiency was calculated by dividing reprogramming efficiencies (D) by plating efficiencies (Figures S1B–S1F). Results are shown as the mean of 3 experiments ± 1 SD.

and day 6). We conclude that any accurate measure of reprogramming potential must account for plating.

Systematic Analysis of Surface Markers

Next we set out to identify additional markers that could be used in conjunction with Thy1, SSEA-1, and *Oct4*-GFP to define stages of reprogramming and further enrich for subsets poised to form iPSCs. For this analysis, we used *Col1a1-tetO-OKSM*^{het} *Rosa26-rtTA*^{het} (het/het) MEFs with an endogenous *Oct4-GFP* reporter. To identify candidate markers, we performed RNA sequencing (RNA-seq) on FACS-purified SSEA-1$^+$ and SSEA-1$^-$ intermediates. We identified a number of genes encoding for cell surface proteins whose expression changes during reprogramming and that are differentially expressed between SSEA-1$^+$ and SSEA-1$^-$ cells. We selected 16 antigens, including previously published markers, for further analysis based on the availability of commercial antibodies for flow cytometry (Figures 2A and S2A). We observed 3 major patterns of marker expression: MEF markers, which are expressed by MEFs and downregulated in SSEA-1$^+$ intermediates; transient markers, which are specifically induced during reprogramming but silenced in iPSCs; and iPSC markers, which are gradually induced during reprogramming and expressed by iPSCs.

Surface protein expression, assessed by flow cytometry, mirrored RNA expression (Figures 2A–2C and S2A–S2C). With respect to MEF markers, platelet derived growth factor receptor β (PDGFRβ) is rapidly downregulated in all intermediates, demonstrating that cells uniformly respond to reprogramming factors. VCAM1 and CD44 are gradually and specifically downregulated in SSEA-1$^+$ intermediates, with VCAM1 being lost before CD44 (Figures 2B and 2C, left). Regarding transient markers, CD73 (*Nt5e*), CD49d (*Itga4*), and Sca-1 (*Ly6a*) are rapidly induced and then silenced prior to *Oct4-GFP* induction. CD73 and Sca-1 are expressed by both SSEA-1$^+$ and SSEA-1$^-$ cells, whereas CD49d is mainly restricted to SSEA-1$^+$ intermediates and is more rapidly silenced (Figures 2B and 2C, center). For iPSC markers, CD71 (*Tfrc*) is initially induced by all cells and then becomes restricted to SSEA-1$^+$ intermediates. EpCAM is first induced on day 6 specifically in SSEA-1$^+$ intermediates. Unlike other iPSC markers, ICAM1 is first expressed by Thy1$^+$ cells and only late in reprogramming by *Oct4*-GFP$^+$ intermediates (Figures 2B and 2C, right). Altogether, these markers identify cellular transitions during the reprogramming process and define the heterogeneity of SSEA-1$^+$ progressing intermediates (Figure 2D).

For markers to have general utility, they must be applicable to other reprogramming systems and conditions. We first analyzed the effects of small molecules that increase reprogramming efficiency (AA, GSKi, and Alk5i) (Bar-Nur et al., 2014; Vidal et al., 2014; Figure S3). SSEA-1 and EpCAM gain as well as VCAM1, Sca-1, CD24, and Podxl loss correlate with reprogramming progression whereas other markers did not. Interestingly, ICAM1 expression appears to be dependent on AA. We next evaluated tail tip fibroblasts (TTFs) derived from neonatal het/het mice. Marker expression is essentially the same as that for MEFs (Figure S4A). Expression of all markers is similar between het/het MEFs and 3/4 MEFs, with the exception of CD49d, which is expressed more highly and for a prolonged period of time in the 3/4 system (Figure S4B). These systems are similar in that they share the *Stemcca* (polycistronic *OKSM*) allele. We therefore tested reprogramming of MEFs infected with individual dox-inducible lentiviruses (LVs) for the 4 factors. Remarkably, all progression markers had similar expression patterns in this system compared with het/het MEFs (Figure S4C). Finally, we analyzed another secondary system, "*OSKM* (Jae)," which differs from *Stemcca* in the stoichiometry of the 4 factors and the *Klf4* isoform (Carey et al., 2011; Kim et al., 2015). These MEFs reprogrammed more slowly and with lower efficiency. They respond to dox induction early by losing PDGFRβ and gaining Podxl, CEACAM1, and Sca-1 (Figure S4D). SSEA-1 is first detectable after day 10 of reprogramming, followed by subsequent expression of CD71, EpCAM, and, finally, c-Kit. This order of marker expression within the SSEA-1$^+$ subset is the same as that in het/het MEFs. We conclude that progression markers are conserved among all examined systems and conditions and, thus, have general applicability.

Revisiting Published Markers

Next, we revisited published markers using the same reprogramming system (3/4 MEFs) and accounting for plating. We first sorted day 3 CD73$^+$ or CD73$^-$ and CD49d$^+$ or CD49d$^-$ intermediates and assessed reprogramming and adjusted reprogramming efficiencies (Figures 3A and 3B). Consistent with Lujan et al. (2015), CD73 and CD49d positivity correlate with reprogramming, yielding plating-adjusted efficiencies of 20%–30%. However, this effect was less striking than that of SSEA-1$^+$ cells, which reached efficiencies of up to 40%. Both CD73 and CD49d subdivide the SSEA-1$^+$ population during early reprogramming. We therefore asked whether the CD73$^+$ or CD49d$^+$ subsets within the day 3 SSEA-1$^+$ populations further enrich for reprogramming potential. Indeed, SSEA-1$^+$CD73$^+$ and SSEA-1$^+$CD49d$^+$ subsets had higher reprogramming efficiencies than their SSEA-1$^+$ marker-negative counterparts on day 3 (Figures 3C, S5A, and S5B). However, although these marker combinations were predictive of successful reprogramming early, they tracked with cells that failed to reprogram at later time points.

Surprisingly, CD49d and, to a lesser extent, CD73 correlate with mCherry levels, suggesting that these markers, unlike Thy1 and SSEA-1, predominantly reflect expression strength of the *OKS* transgene, similar to CD24 (Shakiba et al., 2015; Figure 3D). To determine whether transgene expression correlates with reprogramming efficiency, we sorted SSEA-1$^+$ mCherry^{low} and mCherry^{high} cells and measured adjusted reprogramming efficiencies (Figure 3E). On day 3, higher mCherry levels tracked with increased reprogramming efficiency. However, on day 6, this correlation was gone, similar to our results for CD49d and CD73 (Figures 3C and 3E). CD49d, but not CD73, was more highly expressed during the reprogramming of 3/4 MEFs compared with het/het MEFs (Figures 2B, 2C, and S4B), suggesting that the higher transgene levels in the 3/4 system induce more CD49d expression. To confirm this, we generated MEFs heterozygous or homozygous for *Col1a1-OKSM* and *R26-rtTA* and determined the fraction of CD49d$^+$ cells on day 3 by flow cytometry. Indeed, CD49d expression correlated with expression of the reprogramming factors (Figures 3F and 3G). Finally, we reprogrammed MEFs using individual LVs. On day 3, CD49d expression again corresponded with increased reprogramming factor expression (Figure 3H). Thus, CD49d and CD73 appear

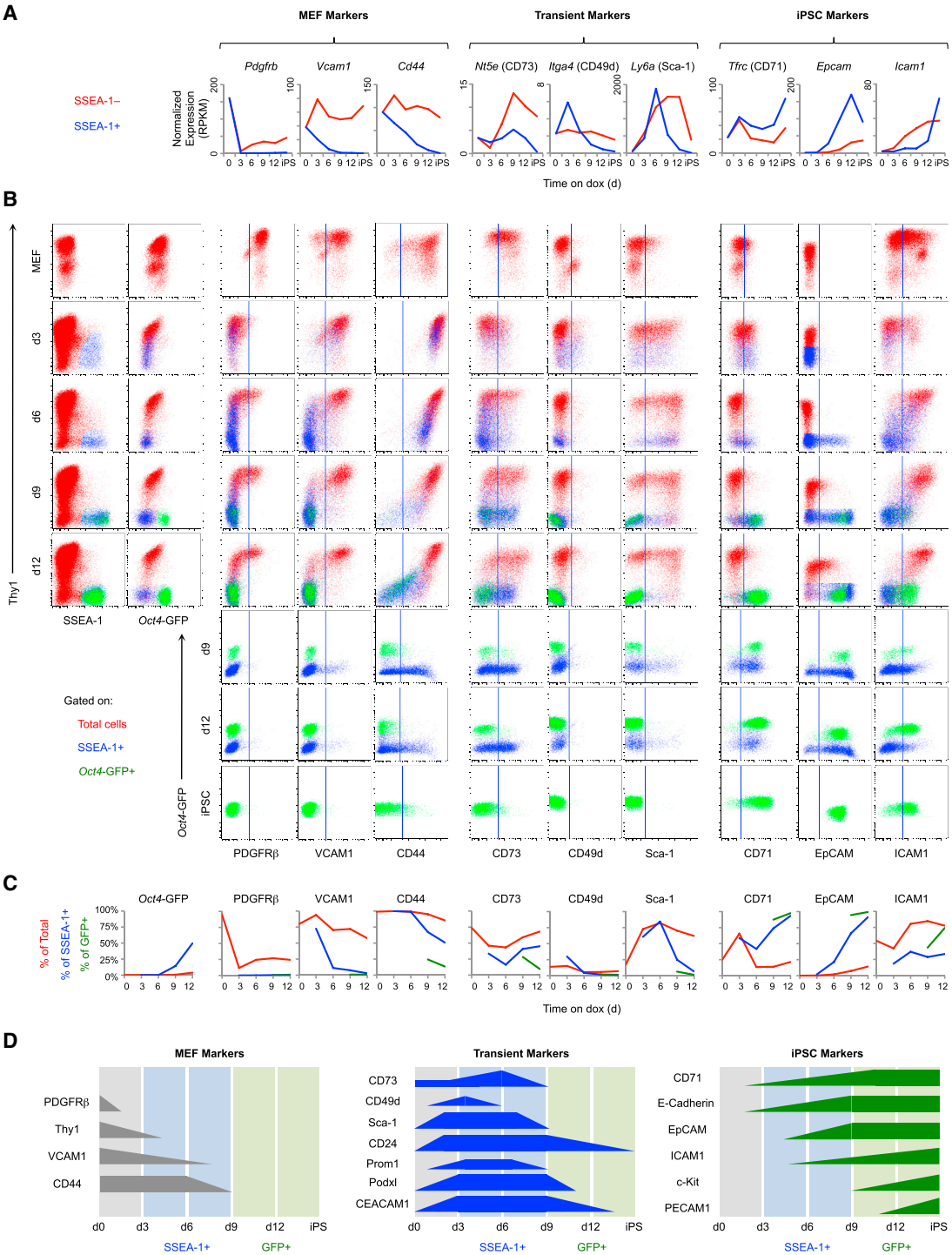

Figure 2. Identification and Characterization of Reprogramming Markers

(A) Transcriptional profiles of candidate cell surface markers. SSEA-1^{-} (red) and SSEA-1^{+} intermediates (blue) derived from het/het MEFs were analyzed by RNA-seq. Results are shown as the mean of 3 replicates.

(B) Flow analysis of het/het MEF reprogramming. Representative dot plots are gated on total live cells (red), SSEA-1^{+} cells (blue), or *Oct4*-GFP^{+} cells (green). Vertical lines indicate the cutoff between negative and positive staining based on an isotype-matched negative control.

(C) Quantification of the plots in (B). Lines show the percentage of total live cells (red), SSEA-1^{+} cells (blue), and *Oct4*-GFP^{+} cells (green) positive for the indicated markers.

(D) Schematic of reprogramming marker expression based on the results above and Figure S2.

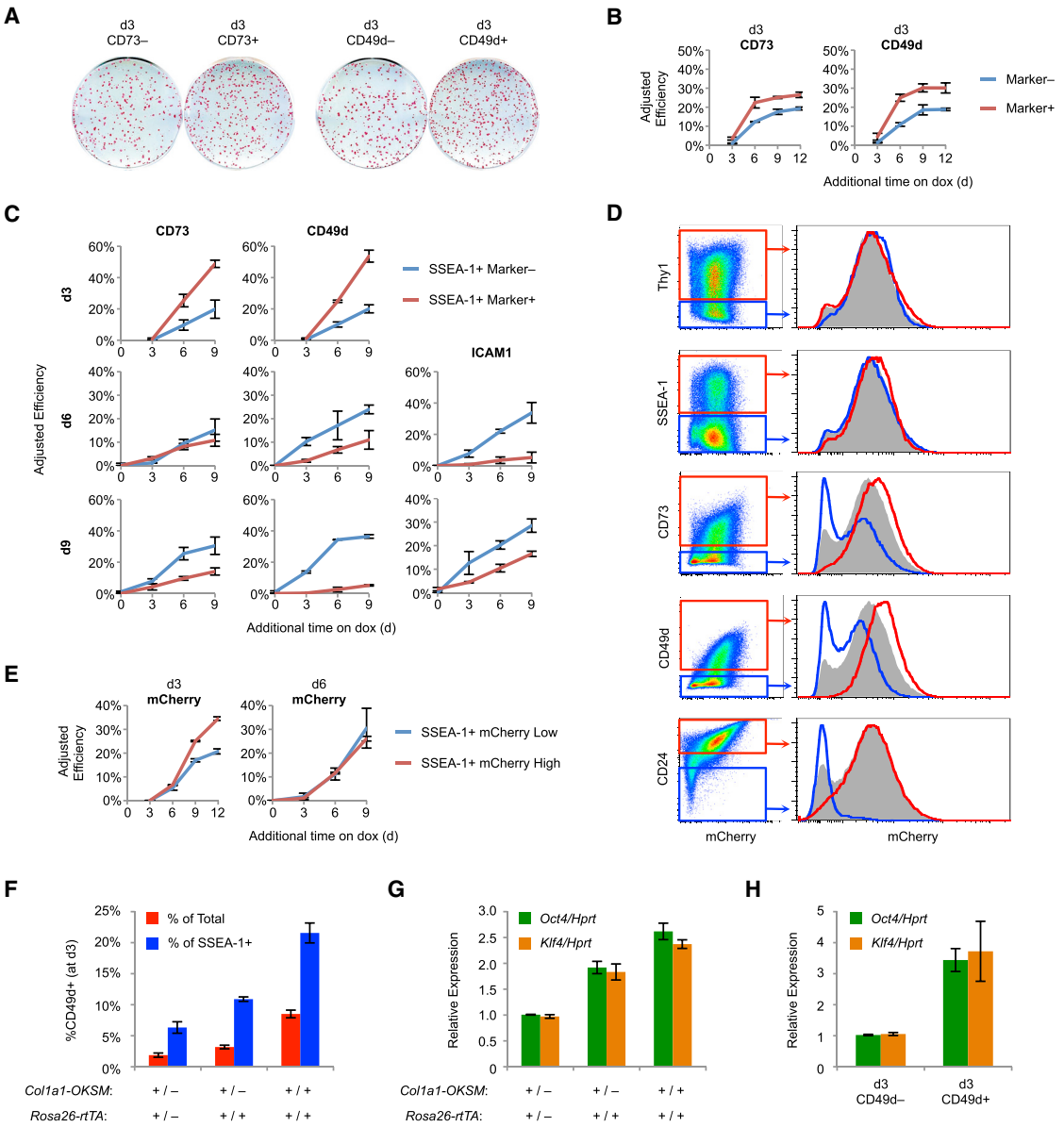

Figure 3. Functional Evaluation of Published Markers

(A) 3/4 MEFs were reprogrammed for 3 days and then sorted for CD73 or CD49d. Shown are AP stains of representative wells exposed to dox for 9 additional days, followed by a period of dox withdrawal.

(B) Adjusted reprogramming efficiencies of day 3 CD73 and CD49d subsets derived from 3/4 MEFs. Results are shown as the mean of 3 experiments ± 1 SD.

(C) Adjusted reprogramming efficiencies of the indicated SSEA-1^{+} subsets derived from 3/4 MEF reprogramming. Results are shown as the mean of 3 experiments ± 1 SD.

(D) Flow analysis for mCherry reporter expression on day 3 of 3/4 MEF reprogramming. Histograms are gated on all cells (gray), marker^{-} cells (blue), or marker^{+} cells (red).

(E) Adjusted reprogramming efficiencies of mCherry^{low} (lowest 25% of mCherry expression) and mCherry^{high} (highest 25% of mCherry expression) SSEA-1^{+} subsets derived from 3/4 MEFs. Results are shown as the mean of 3 experiments ± 1 SD.

(F) MEFs of the indicated genotypes were reprogrammed for 3 days and then analyzed by flow cytometry for SSEA-1 and CD49d expression. Results are shown as the mean of 3 experiments ± 1 SD.

(G) MEFs of the indicated genotypes were reprogrammed for 3 days and then analyzed by qRT-PCR. Results are shown as the mean of 3 experiments ± 1 SD.

(H) MEFs were infected with individual LVs for *OKSM*. On day 3 of reprogramming, intermediates were sorted for CD49d and analyzed by qRT-PCR. Results are shown as the mean of 3 experiments ± 1 SD.

to be early predictive markers of reprogramming as they enrich for cells with high *OKSM* levels. Consistent with this, CD73 and CD49d have been shown to be expressed by partially reprogrammed iPSCs, which remain addicted to high levels of exogenous reprogramming factors (Lujan et al., 2015). This property makes these markers most useful for systems exhibiting heterogeneous expression of *OKSM*.

ICAM1 expression has also been suggested to correlate with reprogramming potential (O'Malley et al., 2013). However, ICAM1 is expressed predominantly by Thy1$^+$ cells, which are refractory to reprogramming (Figures 2A–2C). Although ICAM1 is first expressed on day 6 within the SSEA-1$^+$ population, its expression negatively correlates with adjusted reprogramming efficiencies (Figures 3C, S5A, and S5B). ICAM1 is likely a late marker of reprogramming because *Oct4*-GFP$^+$ intermediates are ICAM1$^+$ (Figures 2A–2C). Altogether, we have systematically compared previously described markers under identical conditions and find that the SSEA-1$^+$ population contains the largest fraction of cells poised to form iPSCs at each time point.

Early Reprogramming Intermediates Poised to Become iPSCs with High Efficiency

The SSEA-1$^+$ population is heterogeneous for VCAM1, Sca-1, CD71, and EpCAM expression early in reprogramming (Figure 2). Consistent with its expression pattern, VCAM1 loss within the SSEA1$^+$ population correlates with increased adjusted reprogramming efficiency (Figures 4A, S5A, and S5B). Sca-1 is a transient marker, suggesting that its upregulation might enrich for cells poised to form iPSCs. Unexpectedly, SSEA-1$^+$Sca-1$^+$ cells are less efficient at reprogramming at every time point analyzed, implying that Sca-1 expression marks an alternative reprogramming route that fails to reach the iPSC fate, whereas Sca-1$^-$ further enriches for cells poised to become iPSCs (Figures 4A, S5A, and S5B). CD71 and EpCAM are both iPSC markers that correlate with reprogramming progression at each time point, with EpCAM$^+$ cells being more efficient than CD71$^+$ cells on day 6 (Figures 4A, S5A, and S5B). Together, these data demonstrate that our markers enable further enrichment for cells poised to become iPSCs when combined with SSEA-1.

We next tested combinations of the aforementioned markers. On day 3, Sca-1, VCAM1, CD73, and CD49d are heterogeneously expressed within the SSEA-1$^+$ population (Figure 4B, top). Critically, SSEA-1$^+$CD73$^+$Sca-1$^-$ emerged as the most efficient combination, with a robust reprogramming potential of ~50% (Figures 4C, left, and S5C). On day 6, many more markers are differentially expressed within the SSEA-1$^+$ population, and there are clear correlations between some of these markers (Figure 4B, bottom). For example, VCAM1$^+$ cells are Sca-1$^+$ and EpCAM$^-$. Therefore, it was not necessary to sort every possible combination. Instead, we focused on EpCAM and Sca-1 expression. Remarkably, the combination of SSEA-1$^+$EpCAM$^+$Sca-1$^-$ resulted in an unprecedented adjusted reprogramming efficiency of ~95%, whereas the other combinations of EpCAM and Sca-1 all had comparatively low reprogramming potentials (Figure 4C, right). Both day 3 efficient (SSEA-1$^+$CD73$^+$Sca-1$^-$) and day 6 efficient (SSEA-1$^+$EpCAM$^+$Sca-1$^-$) intermediates, referred to as "Eff," are extremely rare, comprising ~0.3% of all cells on day 3 and ~0.1% of total cells on day 6 (Figure 4D).

To determine whether day 3 Eff cells preferentially give rise to day 6 Eff cells, we sorted day 3 Eff and day 3 inefficient ("Ineff") cells (SSEA-1$^+$CD73$^-$Sca-1$^+$) and analyzed them after 3 additional days on dox. Indeed, day 3 Eff cells gave rise to ~10 times more EpCAM$^+$Sca-1$^-$ cells than day 3 Ineff cells (Figure S5D), suggesting a direct progression from day 3 Eff to day 6 Eff cells. On day 6, Eff cells are the only intermediates that can generate iPSCs without further dox exposure (Figure 4E); however, this efficiency is extremely low, indicating that the majority of these cells are not yet stably reprogrammed. Finally, all reprogramming systems we analyzed converge on this SSEA-1$^+$EpCAM$^+$Sca-1$^-$ intermediate (Figure S5E). These cells arise prior to endogenous *Oct4-GFP* or *Sox2-GFP* expression, and almost all GFP$^+$ cells are EpCAM$^+$Sca-1$^-$. In summary, we have dissected the heterogeneity of SSEA-1$^+$ intermediates using additional markers and identified the most critical subsets on day 3 and day 6 (Figure 4F). These intermediates are poised to undergo successful reprogramming at unparalleled efficiencies of up to 50% on day 3 and 95% on day 6.

Somatic Extinction Precedes Pluripotency Induction in Poised Intermediates

Poised intermediates are a unique tool to dissect the mechanisms of successful reprogramming. We therefore compared day 3 Eff and day 6 Eff cells molecularly with corresponding day 3 Ineff and day 6 Ineff (SSEA-1$^+$EpCAM$^-$Sca-1$^+$) intermediates as well as the starting MEFs and resulting iPSCs by RNA-seq, assay for transposase-accessible chromatin sequencing (ATAC-seq), and whole genome bisulfite sequencing (WGBS) (Figure 4F). We initially focused on transcriptional analyses to define gene expression patterns that may account for the striking differences in reprogramming potential. Multidimensional scaling (MDS) illustrates a clear trajectory of transcriptional changes that delineates the successful path to reprogramming (Figure 5A). Of note, day 6 Ineff intermediates appear to be stalled and fail to progress beyond day 3 intermediates, whereas day 6 Eff cells proceed toward iPSCs. Consistent with Polo et al. (2012), we observed two waves of transcriptional changes: from MEFs to day 3 SSEA-1$^+$ cells and from day 6 SSEA-1$^+$ cells to iPSCs (Figure 5B; Table S1). Importantly, day 3 Eff cells were more different from MEFs than day 3 Ineff cells, whereas day 6 Eff cells were more similar to iPSCs than day 6 Ineff cells, suggesting that Eff intermediates are more effective at silencing the somatic program on day 3 and activating the pluripotency program at day 6.

Comparing Eff with Ineff intermediates, we detected 264 differentially expressed genes (DEGs) on day 3 and 2,209 DEGs on day 6 (Figures 5B and 5C; Table S2). Most day 3 DEGs (190) overlap with day 6 DEGs, suggesting a progression of transcriptional changes. Hierarchical clustering based on day 3 DEGs segregates MEFs from all other samples, indicating that day 3 DEGs are driven by genes that distinguish reprogramming intermediates and iPSCs from MEFs (Figure 5D, left). By contrast, day 6 DEGs cluster day 6 Eff intermediates with iPSCs, indicating that day 6 Eff but not Ineff cells have initiated an iPSC-specific transcriptional program (Figure 5D, right).

Cell surface markers differentially expressed between Eff and Ineff intermediates (Figure S6A) include genes for CD73, EpCAM, and Sca-1, validating our sorting strategy. Although

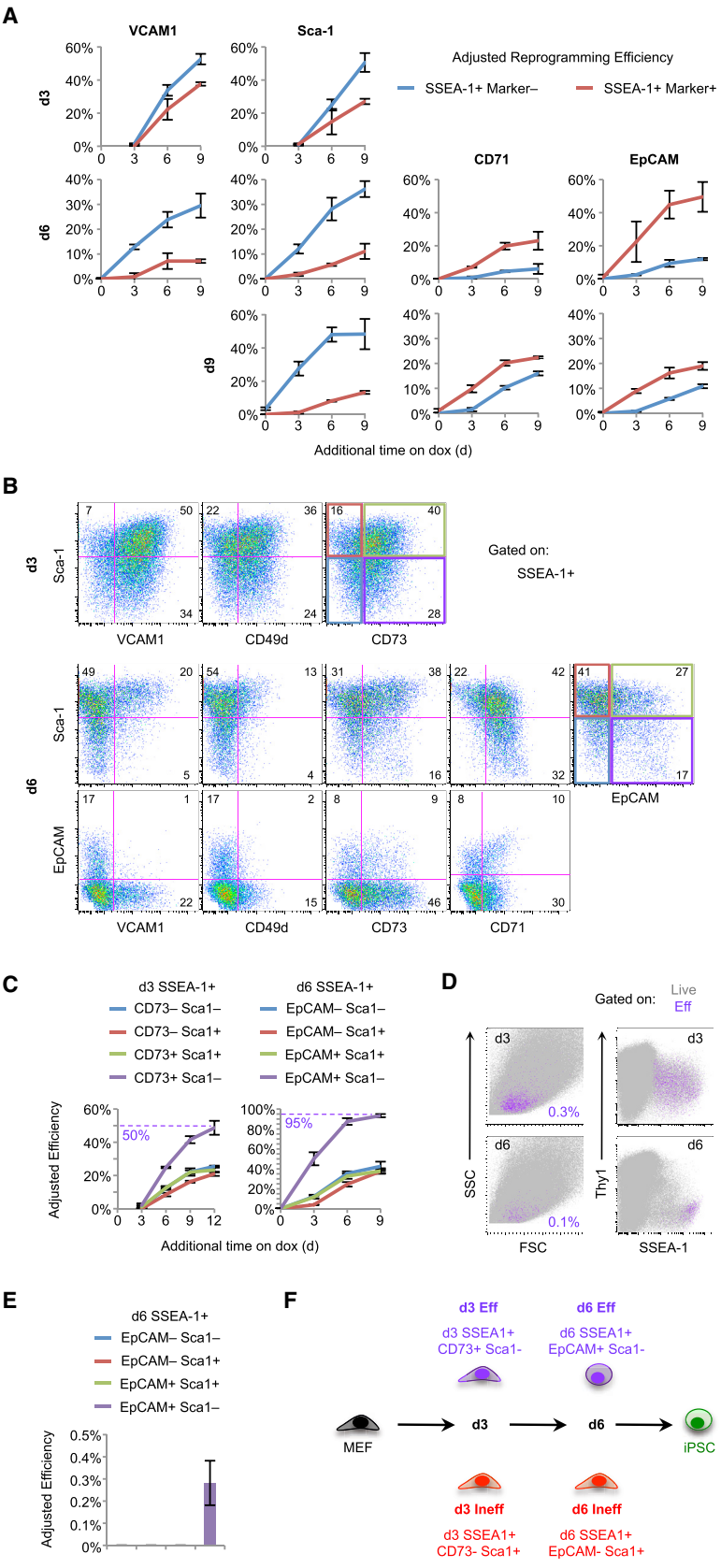

Figure 4. Functional Evaluation of Surface Marker Combinations

(A) Adjusted reprogramming efficiencies of the indicated SSEA-1$^+$ subsets derived from 3/4 MEF reprogramming. Results are shown as the mean of 3 experiments ± 1 SD.

(B) Flow analysis of day 3 (top) and day 6 (bottom) intermediates derived from het/het MEFs. Shown are representative pseudocolor plots gated on SSEA-1$^+$ cells for the indicated markers. Numbers indicate the percentage of cells in each quadrant.

(C) Adjusted reprogramming efficiencies of SSEA-1$^+$ intermediates sorted for the indicated marker combinations on day 3 or day 6 of 3/4 MEF reprogramming. Results are shown as the mean of 3 experiments ± 1 SD.

(D) Overlays of day 3 (top) and day 6 (bottom) Eff cells (purple) on total live cells (gray) derived from het/het MEF reprogramming. Numbers indicate the percentage of Eff cells.

(E) The indicated day 6 SSEA-1$^+$ subsets, derived from 3/4 MEFs, were sorted and replated without dox. Adjusted reprogramming efficiencies are shown as the mean of 3 experiments ± 1 SD.

(F) Summary of the marker combinations used to define Eff and Ineff SSEA-1$^+$ subsets.

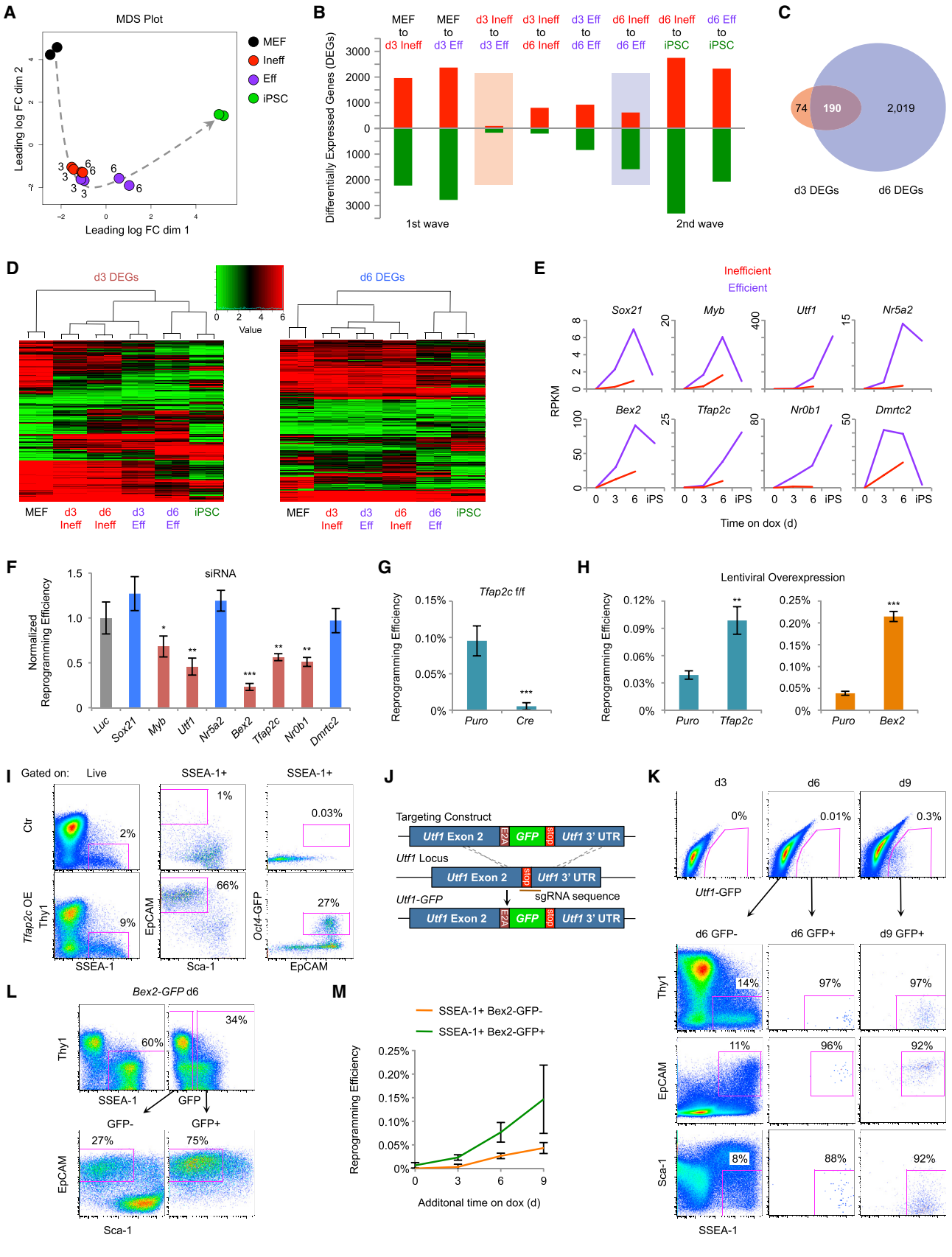

(legend on next page)

Ineff and Eff cells are both SSEA-1$^+$, *Fut9*, which encodes for the enzyme that produces SSEA-1, was more highly expressed by Eff intermediates. Consistent with this observation, SSEA-1 levels positively correlate with adjusted reprogramming efficiencies (Figure S6B). Collectively, these results demonstrate that early transcriptional changes in the select cells poised to successfully reprogram are driven first by effective extinction of the somatic program on day 3 and subsequently by activation of pluripotency loci on day 6.

Identification of TFs Important for the Acquisition of Pluripotency

We next focused on differentially expressed TFs because these may drive differences in reprogramming potential. Several known pluripotency factors were more highly expressed by day 6 Eff compared with day 6 Ineff cells, including *Nanog*, *Prdm14*, *Lin28*, *Zscan10*, *Zfp42*, etc. (Table S2). However, only 11 TFs were more highly expressed in Eff relative to Ineff cells on both day 3 and day 6. We selected 8 for small interfering RNA (siRNA) suppression (Figures 5E and 5F). siRNAs targeting *Myb*, *Utf1*, *Bex2*, *Tfap2c*, and *Nr0b1* significantly reduced reprogramming efficiencies compared with the *Luciferase* control. *Nr5a2*, which can replace *Oct4* in reprogramming (Heng et al., 2010), had no effect in our assay, which may be due to functional redundancy. *Nr0b1* and *Utf1* have established roles in reprogramming (Buganim et al., 2012; Lujan et al., 2015), whereas *Bex2*, *Tfap2c*, and *Myb* may be novel regulators of induced pluripotency.

Tfap2c (aka *Tcfap2c*) encodes for AP-2γ. To validate its functional importance, we reprogrammed *Tfap2c*$^{fl/fl}$ MEFs (Schemmer et al., 2013) with LV-*Stemcca*. Deletion of *Tfap2c* with LV-*Cre* resulted in a profound reduction in reprogramming potential (Figure 5G). Conversely, overexpression (OE) of *Tfap2c* increased reprogramming efficiency (Figure 5H, left; Polo et al., 2012), and this effect was most pronounced in the absence of AA (Figure S6C). Furthermore, *Tfap2c* OE resulted in a striking increase in the fraction of Eff intermediates as well as *Oct4*-GFP$^+$ cells on day 6 (Figure 5I). To corroborate the functional role of *Bex2* in reprogramming, we infected *Bex2* knockout (KO) or littermate control MEFs (Ito et al., 2014) with LV-*Stemcca*. Contrary to our siRNA results, we found no difference in the number of iPSC-like colonies (Figure S6D). We surmise that the high levels of *OKSM* delivered by LV-*Stemcca* compensate for the lack of *Bex2* during reprogramming but cannot exclude other possibilities, including compensation by other brain-expressed X-linked (BEX) factors in the KO or off-target effects of the siRNA. In further agreement with a functional role of *Bex2* during reprogramming, its OE in het/het MEFs greatly improved reprogramming efficiency (Figure 5H, right). Finally, we confirmed that established *Tfap2c* and *Bex2* KO iPSC clones appear normal (Figure S6E), consistent with reports indicating that both genes are dispensable for embryonic stem cell (ESC) maintenance (Auman et al., 2002; Ito et al., 2014; Schemmer et al., 2013). We conclude that *Tfap2c* is critical for reprogramming, whereas *Bex2* enhances reprogramming but is not absolutely required.

To assess whether expression of these TFs corresponds with the emergence of rare intermediates identified by our surface markers, we analyzed reporters for *Utf1* and *Bex2*. Using CRISPR/Cas9 targeting, we generated *Utf1-GFP* knockin reporter ESCs and derivative het/het reprogrammable MEFs (Figure 5J). Although there were no GFP$^+$ cells on day 3 of reprogramming, we detected rare GFP$^+$ cells on day 6, all of which had the immunophenotype of day 6 Eff cells (Figure 5K). We next reprogrammed *Bex2-GFP* MEFs (Ito et al., 2014) and observed a sizable fraction of GFP$^+$ cells by day 6, most of which exhibited the surface markers of day 6 Eff cells (Figure 5L). Significantly, SSEA-1$^+$*Bex2*-GFP$^+$ cells were more efficient than GFP$^-$ cells at generating iPSCs (Figure 5M), confirming that *Bex2* expression marks cells poised to reprogram. In summary, we have identified regulators of reprogramming by

Figure 5. Transcriptional Analysis of Eff Intermediates Reveals Unexplored Regulators of Reprogramming

(A) MDS analysis of global RNA-seq data for the indicated populations, derived from 3/4 MEFs, in duplicate. Numbers indicate the reprogramming time point of intermediates. The dotted arrow shows the proposed trajectory of transcriptional changes.

(B) Quantification of differentially expressed genes (DEGs) that are upregulated (red) or downregulated (green) for the indicated transitions (Table S1).

(C) Venn diagram showing the overlap of day 3 DEGs (comparing day 3 Ineff and day 3 Eff cells) and day 6 DEGs (comparing day 6 Ineff and day 6 Eff cells) (Table S2).

(D) Heatmaps with hierarchical clustering of the 6 populations in duplicate are shown for day 3 DEGs and day 6 DEGs.

(E) Gene expression levels determined by RNA-seq for TFs more highly differentially expressed by Eff compared with Ineff cells on both day 3 and day 6. Results are shown as the mean of two replicates.

(F) The indicated genes were targeted by siRNA transfection of 3/4 MEFs on day 0, day 3, day 6, and day 9 of reprogramming, followed by 3–5 days of dox withdrawal. Results are shown as the mean of 5 experiments ± 1 SD and normalized to a *Luciferase* (*Luc*) siRNA control. Statistical differences compared with *Luc* were determined by unpaired Student's t test; *$p < 0.05$, **$p < 0.005$, ***$p < 0.0005$.

(G) *Tfap2c*$^{fl/fl}$ MEFs were infected with LV-*Stemcca*, *rtTA*, and either *Cre* or a *Puromycin* (*Puro*) control vector. After 15 days of reprogramming, cells were withdrawn from dox for 3–5 days and then stained for AP. Results are shown as the mean of 3 experiments ± 1 SD. Statistical differences were determined by unpaired Student's t test; ***$p < 0.0005$.

(H) Het/het MEFs were infected with LV-*Tfap2c*, *Bex2*, or a *Puro* control. After 12 days of reprogramming, cells were withdrawn from dox for 3–5 days and then stained for AP. Results are shown as the mean of 3 experiments ± 1 SD. Statistical differences were determined by unpaired Student's t test; **$p < 0.005$, ***$p < 0.0005$.

(I) Flow analysis for reprogramming of *Tfap2c* OE and uninfected control MEFs. Shown are representative pseudocolor plots for day 6. The percentages of cells in the indicated regions are shown.

(J) Schematic of the targeting strategy to generate *Utf1-GFP* ESCs.

(K) Flow analysis for reprogramming of *Utf1*-GFP reporter MEFs. Shown are representative pseudocolor plots gated on total live cells (top) and GFP$^-$ or GFP$^+$ intermediates (bottom). The percentages of cells in the indicated regions are shown.

(L) Flow analysis for reprogramming of *Bex2-GFP* reporter MEFs. Shown are representative pseudocolor plots for day 6. Plots are gated on total live cells (top) and GFP$^-$ or GFP$^+$ intermediates (bottom). The percentages of cells in the indicated regions are shown.

(M) Reprogramming efficiency of SSEA-1$^+$*Bex2*-GFP$^-$ and *Bex2*-GFP$^+$ intermediates. Results are shown as the mean of 3 experiments ± 1 SD.

comparing the transcriptional profiles of Eff and Ineff SSEA-1$^+$ subpopulations. The majority of these genes were either not detected at all or only at later stages of reprogramming when analyzing bulk cultures or enriching intermediates solely based on SSEA-1 (Mikkelsen et al., 2008; Polo et al., 2012), highlighting the importance of our high-resolution characterization of progressing intermediates.

Rapid Rewiring of Chromatin States during Reprogramming

Oct4, Sox2, and Klf4 were suggested to act as pioneer factors that initiate cellular reprogramming by binding to closed regions of chromatin, resulting in nucleosome displacement and chromatin remodeling (Soufi et al., 2012). However, because previous studies analyzed bulk cultures that are dominated by cells that fail to reprogram, chromatin changes specific to those rare cells poised to form iPSCs remain unknown. We therefore performed ATAC-seq, which globally quantifies chromatin accessibility (Buenrostro et al., 2013), using our highly enriched intermediates (Figure 4F). Principal-component analysis (PCA) reveals a rapid change in chromatin structure following *OKSM* induction, evident in both day 3 Ineff and Eff cells relative to MEFs, whereas day 6 intermediates are more closely related to iPSCs (Figure 6A). This implies that *OKSM* facilitates transient changes to chromatin accessibility regardless of whether cells progress or stall during reprogramming.

We next analyzed the overlap of ATAC-seq peaks between different populations (Figure 6B). MEF-specific regions are rapidly closed following reprogramming initiation, whereas a large fraction of ectopic peaks (not open in MEFs or iPSCs) are induced in all intermediates. Although most iPSC-specific regions remain closed, "early iPSC" regions are rapidly induced. Significantly, we detected more of these regions in Eff than in Ineff intermediates on both day 3 and day 6 (Figure 6B, inset). Furthermore, day 3 Eff cells undergo chromatin closure for a greater number of MEF regions than day 3 Ineff cells (Figure S6F, left). By contrast, day 6 Eff cells have more open iPSC regions than day 6 Ineff intermediates (Figure S6F, right). We conclude that early changes in chromatin accessibility are driven by silencing of the somatic program on day 3, followed by induction of pluripotency regions on day 6, in agreement with our transcriptional analysis.

Critical Pluripotency Regions Are Hyperaccessible in Poised Intermediates

To narrow down ATAC-seq sites of biological relevance, we considered only differentially accessible regions (DARs) that are open in MEFs (MEF > iPSCs) and remain open in day 3 Ineff cells (day 3 Ineff > day 3 Eff) and day 6 Ineff cells (day 6 Ineff > day 6 Eff), yielding 98 regions (Figure 6C, left; Table S3). Notably, these regions are more open in day 3 Ineff intermediates relative to MEFs and are completely closed in day 6 Eff cells and iPSCs, suggesting that their closure is critical for successful reprogramming (Figure 6D, left). By contrast, 576 DARs are more open in iPSCs (iPSC > MEF), day 3 Eff cells (day 3 Eff > day 3 Ineff), and day 6 Eff cells (day 6 Eff > day 6 Ineff) (Figure 6C, right; Table S3). Surprisingly, Eff intermediates showed increased accessibility compared with iPSCs for these regions (Figure 6D, right), suggesting that a transient hyperaccessible chromatin state at these sites is important for successful reprogramming. Hyperaccessibility had not been previously detected in the analysis of bulk reprogramming cultures or SSEA-1$^+$ intermediates (Chronis et al., 2017; Knaupp et al., 2017; Li et al., 2017), further underscoring the importance of evaluating poised reprogramming subsets.

The 576 DARs more open in iPSCs and Eff intermediates include hyperaccessible peaks adjacent to a number of key pluripotency genes (Figure 6E; Table S3). These encompass genes more highly expressed by Eff cells on both day 3 and day 6 (*Bex2*, *Tfap2c*, *Nr0b1*, *Nr5a2*, and *Mycn*) as well as genes not expressed until day 6 or later (*Prdm14* and *Zscan10*). Of particular interest was the region adjacent to *Dppa3* (Figure S7A), which maps to a known super-enhancer (−45 super-enhancer [SE]) that controls the expression of both *Dppa3* and *Nanog* (Blinka et al., 2016). Despite the apparent activation of this enhancer as early as day 3, *Nanog* is not expressed until day 6, specifically by Eff intermediates, and *Dppa3* is not expressed until even later. This observation therefore implies that changes to chromatin accessibility, particularly hyperaccessibility, can precede and may be causal to changes in gene expression.

To ascertain which TFs might bind to the 576 DARs more accessible in Eff intermediates and iPSCs, we performed TF motif enrichment analysis. Top hits included Klf4 ($p = 7.16 \times 10^{-60}$) and Oct4/Sox2 ($p = 1.09 \times 10^{-53}$), suggesting that these regions are enriched for direct binding sites of the reprogramming factors. Thus, hyperaccessibility might be due to superphysiological levels of *OKS*. However, Eff intermediates expressed less or equal amounts of *OKS* compared with endogenous levels in iPSCs, arguing against this possibility (Figure S6G). To verify OKS binding to these hyperaccessible loci, we analyzed ESC chromatin immunoprecipitation sequencing (ChIP-seq) data for Oct4, Sox2, and Klf4 (Chronis et al., 2017). Most of the hyperaccessible sites were indeed bound by OKS (Figures 6E and S6H). Furthermore, 70% of these sites were occupied by a combination of Oct4 and Sox2 ± Klf4, suggesting that cooperative binding may be responsible for hyperaccessibility. Examples include two peaks upstream of *Mybl2*, the peak between *Dppa3* and *Nanog*, and a peak adjacent to *Tfap2c* (Figures 6F, S7A, and S7B). However, we also identified rare DARs not bound by any reprogramming factors, such as the promoter region of *Bex2* (Figures 6E, S6H, and S7C). Motif analysis for this peak suggested a Tfap2c binding site, which was confirmed by published ChIP-seq data (Park et al., 2015). We conclude that regions of hyperaccessibility, revealed only by dissecting the rare intermediates poised to reprogram, identify key *cis*-regulatory elements critical for reprogramming.

DNA Methylation and Demethylation Are Uncoupled during Reprogramming

DNA methylation provides another layer of epigenetic regulation. Reprogramming requires demethylation of pluripotency promoters and enhancers, whereas MEF-specific *cis*-regulatory elements are remethylated (Koche et al., 2011). Previous studies of bulk or SSEA-1$^+$ intermediates suggest that DNA methylation changes occur late in reprogramming (Knaupp et al., 2017; Lee et al., 2014; Mikkelsen et al., 2008; Milagre et al., 2017; Polo et al., 2012). To evaluate the dynamics of DNA methylation in our poised intermediates, we performed WGBS (Figure 4F).

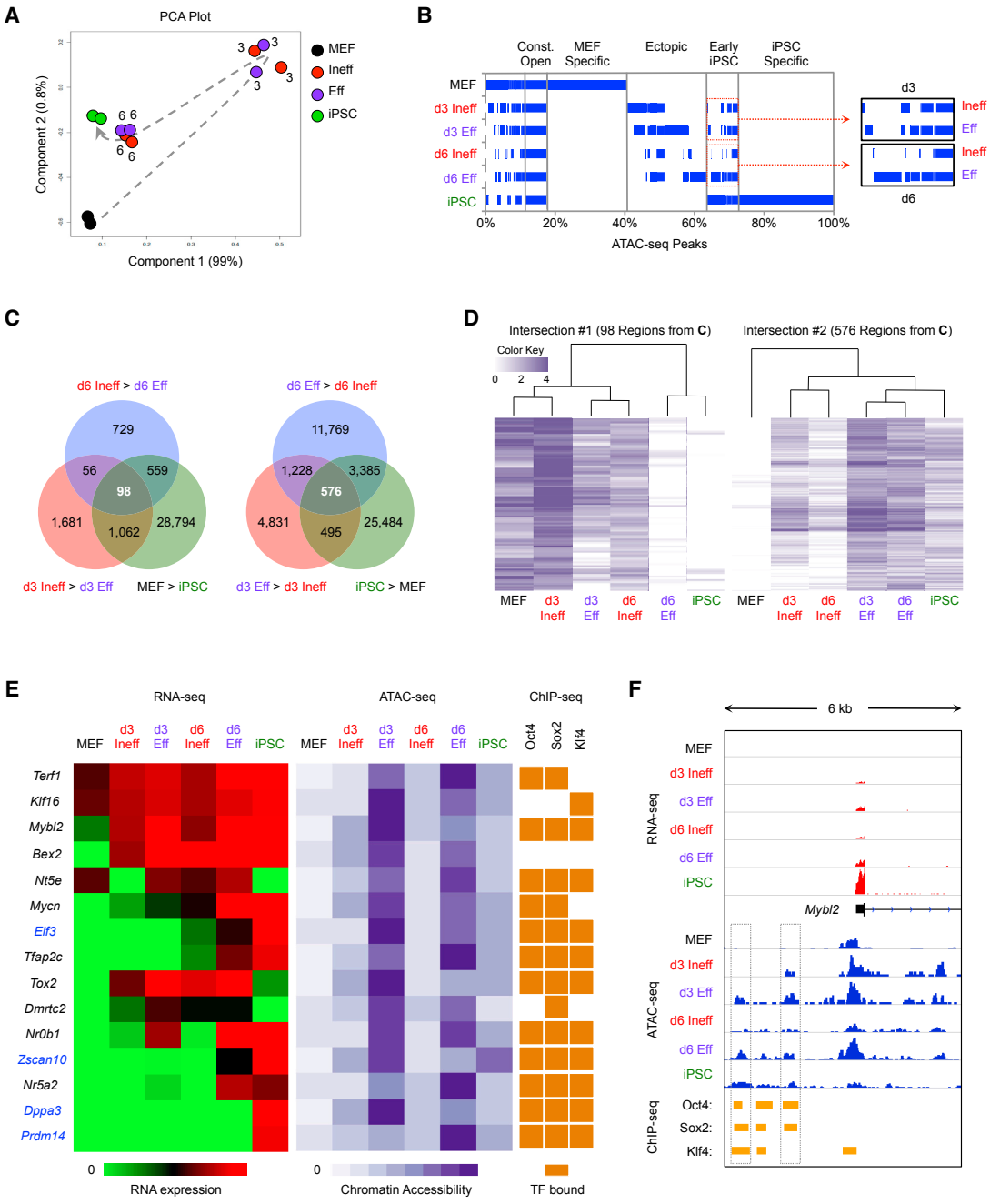

Figure 6. Eff Intermediates Rapidly Acquire Regions of Chromatin Hyperaccessibility

(A) ATAC-seq was performed on the indicated populations in duplicate. Shown is a PCA based on peaks identified in MEFs. Numbers indicate the reprogramming time point of intermediates. The dotted arrow indicates the proposed trajectory of chromatin accessibility changes during reprogramming.

(B) Overlap of ATAC-seq peaks between populations. The percentage of total peaks for every possible combination of overlap is shown. Blue bars represent the presence of peaks in the indicated population(s), whereas white denotes the absence of peaks.

(C) Venn diagram showing the overlap of day 3 differentially accessible regions (DARs) (comparing day 3 Ineff and day 3 Eff cells) and day 6 DARs (comparing day 6 Ineff and day 6 Eff cells) and DARs between MEFs and iPSCs (Table S3).

(D) Heatmaps with hierarchical clustering shown for the indicated sets of DARs from (C). White bars indicate regions of closed chromatin, and darker bars indicate regions with greater chromatin accessibility.

(E) Correlation between gene expression, chromatin accessibility, and TF binding. Regions were selected from intersection #2 (576 ATAC-seq peaks, C) and associated with the closest gene (Table S3). Shown are heatmaps for RNA-seq (left), ATAC-seq (center), and published ChIP-seq for OKS binding in ESCs (Chronis et al., 2017) (right). For genes highlighted in blue, chromatin accessibility precedes transcription.

(F) Genome browser view of RNA-seq (red) ATAC-seq (blue) and ChIP-seq (orange) for the region adjacent to *Mybl2*. Boxes denote areas that are more differentially open by ATAC-seq in day 3 Eff cells, day 6 Eff cells, and iPSCs compared with day 3 Ineff cells, day 6 Ineff cells, and MEFs, respectively.

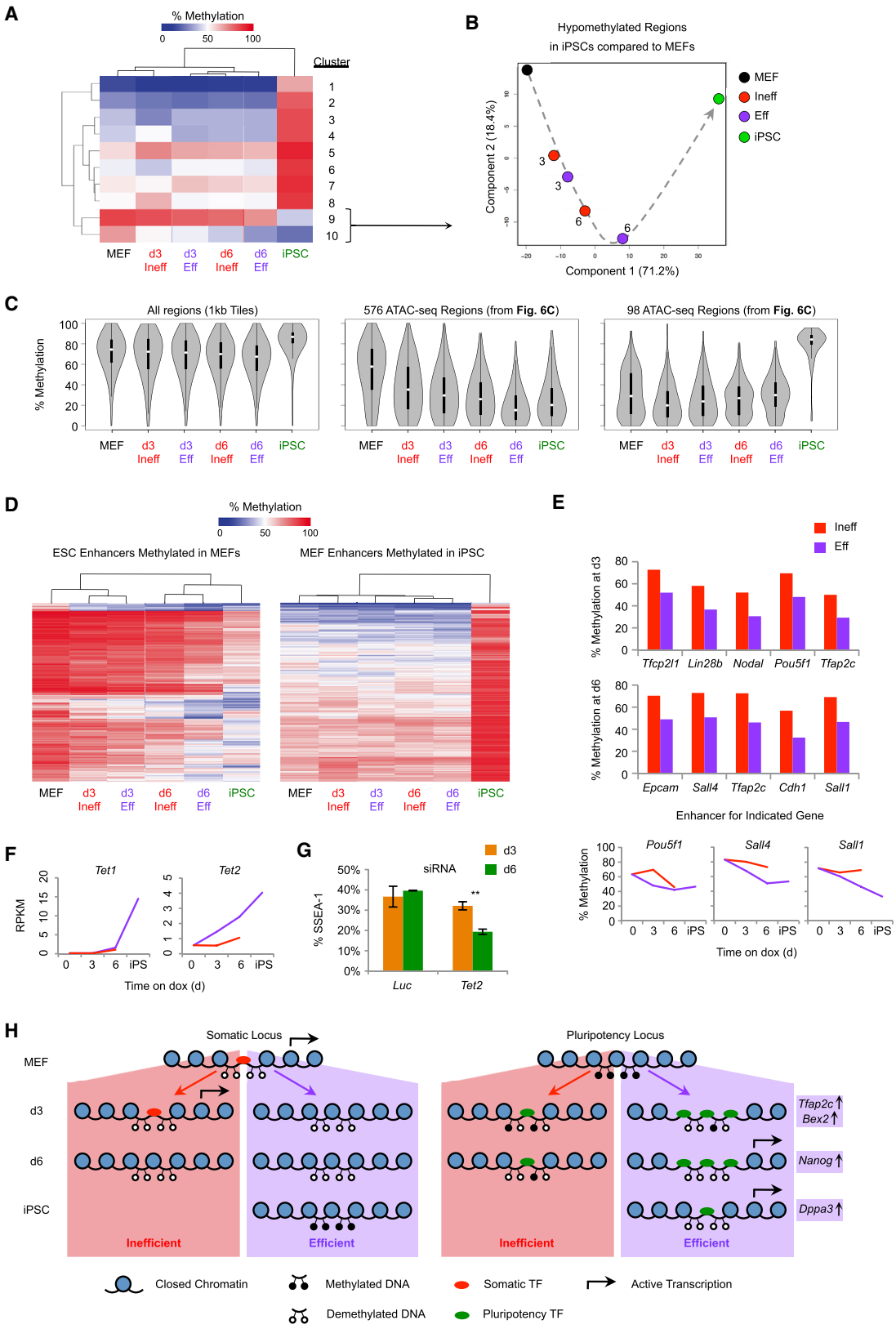

(legend on next page)

Globally, MEFs and intermediates have similar DNA methylation levels, whereas iPSCs are relatively hypermethylated and cluster separately (Figure 7A), consistent with previous observations (Lee et al., 2014; Milagre et al., 2017; Polo et al., 2012). For regions that become methylated specifically in iPSCs, there were only subtle differences among early intermediates (Figure 7A, clusters 1–8), confirming that *de novo* DNA methylation is a late event. Consistent with this, DNMT3A and DNMT3B, which catalyze *de novo* DNA methylation, are not required for reprogramming (Pawlak and Jaenisch, 2011). For regions that are hypomethylated in iPSCs relative to MEFs, we detected two clusters that undergo either immediate or delayed demethylation (Figure 7A, clusters 9 and 10), implying two separable waves of demethylation. Cluster 9 contains DNA regions that are demethylated late in reprogramming and includes regions closest to the promoters of *Zfp42*, *Dppa2*, and *Dppa4*, whereas cluster 10 is composed of regions that are rapidly demethylated, including areas adjacent to *Oct4*, *Klf4*, and *Nanog*, revealing a previously unexplored early wave of demethylation (Table S4). Importantly, day 6 Eff cells were more demethylated than the other reprogramming intermediates (Figure 7A), linking DNA demethylation of specific loci with increased reprogramming efficiency. In support of this observation, PCA for regions in these two clusters demonstrates a clear trajectory of DNA methylation changes during reprogramming (Figure 7B).

We assumed that the earliest regions of chromatin opening would be at areas of DNA hypomethylation in the starting MEFs, allowing for rapid binding of reprogramming factors (Koche et al., 2011). Surprisingly, DARs more accessible in day 3 Eff cells, day 6 Eff cells, and iPSCs are hypermethylated in MEFs but rapidly demethylated on day 3, further demethylated in day 6 Eff cells, and remain demethylated in iPSCs (Figure 7C, center). Conversely, DARs more open in MEFs, day 3 Ineff cells, and day 6 Ineff cells are hypomethylated in MEFs and undergo methylation only late in reprogramming (Figure 7C, right). Next we analyzed sets of annotated enhancers defined in ESCs or MEFs (Shen et al., 2012). For ESC enhancers methylated in MEFs, day 3 intermediates remain predominantly hypermethylated and cluster with MEFs, whereas day 6 intermediates are hypomethylated and cluster with iPSCs, with day 6 Eff cells being the most demethylated (Figure 7D, left). Specific differentially methylated regions (DMRs) less methylated in day 3 Eff cells compared with Ineff cells include enhancers for *Oct4*, *Lin28b*, *Nodal*, *Tfcp2l1*, and *Tfap2c*, whereas DMRs less methylated in day 6 Eff cells compared with Ineff cells include enhancers for *Epcam*, *Cdh1*, *Sall1*, *Sall4*, and *Tfap2c* (Figure 7E; Table S5). Of note, endogenous *Oct4* is not expressed until day 9 (Figures 2B and 2C), implying that specific demethylation of enhancers in Eff intermediates can precede transcription. For MEF enhancers that are methylated in iPSCs, all intermediates were hypomethylated, further demonstrating that *de novo* methylation is not required for the silencing of MEF genes early in reprogramming (Figure 7D, right).

DNA demethylation is mediated, in part, by ten-eleven translocation (TET) enzymes (Koh et al., 2011). *Tet2*, but not *Tet1*, is upregulated early in reprogramming specifically in Eff intermediates (Figure 7F). To determine whether *Tet2* plays a functional role in the formation of Eff intermediates, we transfected cells with siRNA targeting *Tet2*. Although we observed no effect on day 3, we detected a significant reduction in SSEA-1$^+$ reprogramming intermediates on day 6, suggesting an important role for *Tet2* in reprogramming between day 3 and day 6, coinciding with the early wave of DNA demethylation we detected (Figure 7G). We conclude that DNA methylation and demethylation are uncoupled during reprogramming. Additionally, our analysis of highly enriched poised reprogramming intermediates has allowed us to uncover a previously unobserved early wave of DNA demethylation.

DISCUSSION

Here we describe cell surface marker combinations allowing us to prospectively isolate and characterize rare intermediates poised to generate iPSCs with unprecedented efficiencies in the absence of additional treatments. Molecular dissection of these key intermediates elucidates transcriptional and epigenetic events specific to early stages of TF-induced pluripotency (Figure 7H). Altogether, our study provides a valuable resource of surface markers to delineate the various stages of cellular reprogramming and associated transcriptional, chromatin accessibility, and DNA methylation patterns. Our results highlight the importance of controlling for differential plating. We found that reprogramming intermediates are particularly sensitive to the stress of dissociation and cell sorting, resulting in very poor re-plating potentials. This most likely masked the importance of EpCAM as a marker of reprogramming progression in prior studies (Lujan et al., 2015; Polo et al., 2012). Remarkably, our data show that EpCAM expression, in combination with SSEA-1 expression

Figure 7. DNA Methylation and Demethylation Are Uncoupled during Reprogramming

(A) WGBS was performed on the indicated populations. Shown is a heatmap of 1-kb tiling regions that show a change of at least 30% between MEFs and iPSCs as measured by WGBS. Regions were grouped into ten clusters based on hierarchical clustering.

(B) PCA of WGBS data using 1-kb DNA tiles that are hypomethylated in iPSCs relative to MEFs (clusters 9 and 10, A). Numbers indicate the reprogramming time point of intermediates. The dotted arrow indicates the proposed trajectory of DNA methylation changes during reprogramming.

(C) Violin plots of global DNA methylation for the indicated regions. Plots show the distribution of methylation values for each sample. White circle, median methylation value; black box, interquartile range. Whiskers extend to the most extreme data point, which is no more than 1.5 times the interquartile range from the box.

(D) Heatmaps showing DNA methylation levels at ESC enhancers (Shen et al., 2012) that are hypermethylated in MEFs compared with iPSCs (left) and MEF enhancers that are hypomethylated in MEFs compared with iPSCs (right).

(E) DNA methylation levels for key ESC enhancers differentially methylated on day 3 (top) or day 6 (center) of reprogramming (Table S5).

(F) Gene expression levels determine by RNA-seq for *Tet1* and *Tet2*. Results are shown as the mean of two replicates (red line, Ineff; purple line, Eff).

(G) 3/4 MEFs were transfected with siRNA targeting *Tet2* or a *Luc* control on day 0 and day 3 of reprogramming. On day 3 (orange) or day 6 (green), the percentage of SSEA-1$^+$ cells was determined by flow cytometry. Results are shown as the mean of 3 experiments ± 1 SD. Statistical differences were determined by unpaired Student's t test; $^{**}p < 0.005$.

(H) Model of chromatin changes observed in Eff and Ineff intermediates during reprogramming.

and Sca-1 loss, enriches for select intermediates poised to reprogram with nearly 95% efficiency. Furthermore, our study resolves controversies regarding the utility of various cell surface markers to track reprogramming intermediates (Brambrink et al., 2008; Lujan et al., 2015; O'Malley et al., 2013; Stadtfeld et al., 2008). We surmise that these discrepancies are likely due to the use of distinct reprogramming systems. Importantly, our study compares markers in parallel across distinct reprogramming systems and conditions. We confirm that SSEA-1 is an early and robust marker of reprogramming progression. Likewise, we corroborate CD73 and CD49d as early markers. However, instead of signifying progression, these markers correlate with exogenous reprogramming factor expression. Furthermore, CD73 and CD49d switch to negatively predictive markers later in reprogramming, limiting their general utility. Surprisingly, we find that expression of ICAM1 is dependent on AA and is first induced in reprogramming-refractory intermediates and, thus, may not be a predictive marker until late time points.

Transcriptional analysis reveals that *Tfap2c* and *Bex2* are induced specifically in Eff intermediates by day 3, representing two of the earliest transcriptional regulators of successful reprogramming. Intriguingly, both genes are adjacent to *cis* elements that become hyperaccessible exclusively in Eff intermediates. Furthermore, enhancers of *Tfap2c* become specifically demethylated in Eff cells. Consistent with a functional role, *Tfap2c* KO MEFs are significantly impaired in the formation of iPSCs, whereas *Tfap2c* OE augments reprogramming, corroborating our earlier findings (Polo et al., 2012). *Bex2*, on the other hand, is dispensable for reprogramming with high levels of *OKSM*, but OE increases the reprogramming potential. Additionally, activation of endogenous *Bex2* correlates well with cells poised to produce iPSCs. Although *Bex2* and *Tfap2c* are both expressed in pluripotent cell lines, neither is required for ESC self-renewal (Auman et al., 2002; Ito et al., 2014; Schemmer et al., 2013). Our observations provide the basis for future studies aimed at dissecting the mechanisms by which these underexplored TFs specifically facilitate the acquisition but not maintenance of pluripotency.

Our study uncovers that ectopic chromatin accessibility as well as chromatin hyperaccessibility are previously unrecognized hallmarks of successful reprogramming. These data suggest that adoption of an ESC-like chromatin state is insufficient to acquire a stable iPSC state. Instead, a genome-wide increase in chromatin accessibility, combined with focused hyperaccessibility at critical pluripotency loci, correlates with successful reprogramming in our system. Further work remains to determine how these changes in chromatin accessibility correlate with remodeling of histone marks and rewiring of 3D chromatin architecture, both of which can precede transcription (Apostolou et al., 2013; Polo et al., 2012), similar to what we found for hyperaccessibility.

Finally, our study redefines the molecular dynamics of DNA methylation changes during TF-induced cellular reprogramming. Global analysis of our highly enriched intermediates revealed no overall change in DNA methylation levels. However, when focusing specifically on regions that are demethylated in iPSCs, we were able to uncover two distinct waves of demethylation, including a previously unappreciated early wave most evident in our Eff intermediates. On the other hand, *de novo* methylation of somatic regions occurs only late, demonstrating that demethylation and remethylation are uncoupled during reprogramming. Furthermore, a comparison of ATAC-seq with WGBS data revealed that regions of chromatin that are hyperaccessible in Eff intermediates are targeted for rapid DNA demethylation, directly linking these two epigenetic processes. We conclude that key molecular changes occur very early in reprogramming but are typically obscured by the overwhelming majority of cells that do not effectively contribute to the generation of iPSCs.

STAR★METHODS

Detailed methods are provided in the online version of this paper and include the following:

- KEY RESOURCES TABLE
- CONTACT FOR REAGENT AND RESOURCE SHARING
- EXPERIMENTAL MODEL AND SUBJECT DETAILS
  - Animal Care
  - Fibroblast Derivation
- METHOD DETAILS
  - Cell Culture and Reprogramming
  - Flow Cytometry and Cell Sorting
  - Assay for Adjusted Reprogramming Efficiency
  - qRT-PCR
  - RNA-seq
  - ATAC-seq
  - Whole Genome Bisulfite Sequencing (WGBS)
  - siRNA Transfection and Analysis
  - Lentivirus Production and Infections
  - Generation of *Utf1* Reporter Cells
- QUANTIFICATION AND STATISTICAL ANALYSIS
  - Statistical Analysis
  - RNA-seq
  - ATAC-seq
  - WGBS
- DATA AND SOFTWARE AVAILABILITY

SUPPLEMENTAL INFORMATION

Supplemental Information includes seven figures and five tables and can be found with this article online at https://doi.org/10.1016/j.stem.2018.06.013.

ACKNOWLEDGMENTS

We thank Susan Schwarz, Bruno Di Stefano, and members of the Hochedlinger laboratory; Maris Handley and Meredith Weglarz of the MGH CRM/HSCI Flow Core; and members of the MGH Next Generation Sequencing Core. B.A.S. was supported through an MGH Pathology grant (NIH T32 CA921633) and an MGH ECOR fellowship; A.M., by the NIH (P01 GM099117 and P50 HG006193) and the Max Planck Society; R.I.S. by NIH P30 DK40561; and K.H., by funds from MGH, the NIH (R01 HD058013 and P01 GM099134), and the Gerald and Darlene Jordan Chair in Regenerative Medicine.

AUTHOR CONTRIBUTIONS

B.A.S., A.M., and K.H. designed the study. B.A.S., R.M.W., S.C., and H.G. performed and analyzed the experiments. J.L., A.K., and H.S. provided specific MEF lines. M.C., K.C., and R.I.S. performed the bioinformatics analysis. B.A.S. and K.H. wrote the manuscript.

DECLARATION OF INTERESTS

The authors declare no conflicting interests.

Received: September 1, 2017
Revised: March 29, 2018
Accepted: June 15, 2018
Published: July 12, 2018

REFERENCES

Anders, S., Pyl, P.T., and Huber, W. (2015). HTSeq–a Python framework to work with high-throughput sequencing data. Bioinformatics *31*, 166–169.

Apostolou, E., Ferrari, F., Walsh, R.M., Bar-Nur, O., Stadtfeld, M., Cheloufi, S., Stuart, H.T., Polo, J.M., Ohsumi, T.K., Borowsky, M.L., et al. (2013). Genome-wide chromatin interactions of the Nanog locus in pluripotency, differentiation, and reprogramming. Cell Stem Cell *12*, 699–712.

Auman, H.J., Nottoli, T., Lakiza, O., Winger, Q., Donaldson, S., and Williams, T. (2002). Transcription factor AP-2γ is essential in the extra-embryonic lineages for early postimplantation development. Development *129*, 2733–2747.

Bar-Nur, O., Brumbaugh, J., Verheul, C., Apostolou, E., Pruteanu-Malinici, I., Walsh, R.M., Ramaswamy, S., and Hochedlinger, K. (2014). Small molecules facilitate rapid and synchronous iPSC generation. Nat. Methods *11*, 1170–1176.

Blinka, S., Reimer, M.H., Jr., Pulakanti, K., and Rao, S. (2016). Super-enhancers at the Nanog locus differentially regulate neighboring pluripotency-associated genes. Cell Rep. *17*, 19–28.

Brambrink, T., Foreman, R., Welstead, G.G., Lengner, C.J., Wernig, M., Suh, H., and Jaenisch, R. (2008). Sequential expression of pluripotency markers during direct reprogramming of mouse somatic cells. Cell Stem Cell *2*, 151–159.

Buenrostro, J.D., Giresi, P.G., Zaba, L.C., Chang, H.Y., and Greenleaf, W.J. (2013). Transposition of native chromatin for fast and sensitive epigenomic profiling of open chromatin, DNA-binding proteins and nucleosome position. Nat. Methods *10*, 1213–1218.

Buganim, Y., Faddah, D.A., Cheng, A.W., Itskovich, E., Markoulaki, S., Ganz, K., Klemm, S.L., van Oudenaarden, A., and Jaenisch, R. (2012). Single-cell expression analyses during cellular reprogramming reveal an early stochastic and a late hierarchic phase. Cell *150*, 1209–1222.

Carey, B.W., Markoulaki, S., Hanna, J.H., Faddah, D.A., Buganim, Y., Kim, J., Ganz, K., Steine, E.J., Cassady, J.P., Creyghton, M.P., et al. (2011). Reprogramming factor stoichiometry influences the epigenetic state and biological properties of induced pluripotent stem cells. Cell Stem Cell *9*, 588–598.

Chronis, C., Fiziev, P., Papp, B., Butz, S., Bonora, G., Sabri, S., Ernst, J., and Plath, K. (2017). Cooperative binding of transcription factors orchestrates reprogramming. Cell *168*, 442–459.e20.

Dobin, A., Davis, C.A., Schlesinger, F., Drenkow, J., Zaleski, C., Jha, S., Batut, P., Chaisson, M., and Gingeras, T.R. (2013). STAR: ultrafast universal RNA-seq aligner. Bioinformatics *29*, 15–21.

Gifford, C.A., Ziller, M.J., Gu, H., Trapnell, C., Donaghey, J., Tsankov, A., Shalek, A.K., Kelley, D.R., Shishkin, A.A., Issner, R., et al. (2013). Transcriptional and epigenetic dynamics during specification of human embryonic stem cells. Cell *153*, 1149–1163.

Heng, J.C., Feng, B., Han, J., Jiang, J., Kraus, P., Ng, J.H., Orlov, Y.L., Huss, M., Yang, L., Lufkin, T., et al. (2010). The nuclear receptor Nr5a2 can replace Oct4 in the reprogramming of murine somatic cells to pluripotent cells. Cell Stem Cell *6*, 167–174.

Ito, K., Yamazaki, S., Yamamoto, R., Tajima, Y., Yanagida, A., Kobayashi, T., Kato-Itoh, M., Kakuta, S., Iwakura, Y., Nakauchi, H., and Kamiya, A. (2014). Gene targeting study reveals unexpected expression of brain-expressed X-linked 2 in endocrine and tissue stem/progenitor cells in mice. J. Biol. Chem. *289*, 29892–29911.

John, S., Sabo, P.J., Thurman, R.E., Sung, M.H., Biddie, S.C., Johnson, T.A., Hager, G.L., and Stamatoyannopoulos, J.A. (2011). Chromatin accessibility pre-determines glucocorticoid receptor binding patterns. Nat. Genet. *43*, 264–268.

Kim, S.I., Oceguera-Yanez, F., Hirohata, R., Linker, S., Okita, K., Yamada, Y., Yamamoto, T., Yamanaka, S., and Woltjen, K. (2015). KLF4 N-terminal variance modulates induced reprogramming to pluripotency. Stem Cell Reports *4*, 727–743.

Knaupp, A.S., Buckberry, S., Pflueger, J., Lim, S.M., Ford, E., Larcombe, M.R., Rossello, F.J., de Mendoza, A., Alaei, S., Firas, J., et al. (2017). Transient and Permanent Reconfiguration of Chromatin and Transcription Factor Occupancy Drive Reprogramming. Cell Stem Cell *21*, 834–845.e6.

Koche, R.P., Smith, Z.D., Adli, M., Gu, H., Ku, M., Gnirke, A., Bernstein, B.E., and Meissner, A. (2011). Reprogramming factor expression initiates widespread targeted chromatin remodeling. Cell Stem Cell *8*, 96–105.

Koh, K.P., Yabuuchi, A., Rao, S., Huang, Y., Cunniff, K., Nardone, J., Laiho, A., Tahiliani, M., Sommer, C.A., Mostoslavsky, G., et al. (2011). Tet1 and Tet2 regulate 5-hydroxymethylcytosine production and cell lineage specification in mouse embryonic stem cells. Cell Stem Cell *8*, 200–213.

Lee, D.S., Shin, J.Y., Tonge, P.D., Puri, M.C., Lee, S., Park, H., Lee, W.C., Hussein, S.M., Bleazard, T., Yun, J.Y., et al. (2014). An epigenomic roadmap to induced pluripotency reveals DNA methylation as a reprogramming modulator. Nat. Commun. *5*, 5619.

Li, D., Liu, J., Yang, X., Zhou, C., Guo, J., Wu, C., Qin, Y., Guo, L., He, J., Yu, S., et al. (2017). Chromatin Accessibility Dynamics during iPSC Reprogramming. Cell Stem Cell *21*, 819–833.e6.

Li, H., and Durbin, R. (2009). Fast and accurate short read alignment with Burrows-Wheeler transform. Bioinformatics *25*, 1754–1760.

Lujan, E., Zunder, E.R., Ng, Y.H., Goronzy, I.N., Nolan, G.P., and Wernig, M. (2015). Early reprogramming regulators identified by prospective isolation and mass cytometry. Nature *521*, 352–356.

Mikkelsen, T.S., Hanna, J., Zhang, X., Ku, M., Wernig, M., Schorderet, P., Bernstein, B.E., Jaenisch, R., Lander, E.S., and Meissner, A. (2008). Dissecting direct reprogramming through integrative genomic analysis. Nature *454*, 49–55.

Milagre, I., Stubbs, T.M., King, M.R., Spindel, J., Santos, F., Krueger, F., Bachman, M., Segonds-Pichon, A., Balasubramanian, S., Andrews, S.R., et al. (2017). Gender differences in global but not targeted demethylation in iPSC reprogramming. Cell Rep. *18*, 1079–1089.

O'Malley, J., Skylaki, S., Iwabuchi, K.A., Chantzoura, E., Ruetz, T., Johnsson, A., Tomlinson, S.R., Linnarsson, S., and Kaji, K. (2013). High-resolution analysis with novel cell-surface markers identifies routes to iPS cells. Nature *499*, 88–91.

Park, J.M., Wu, T., Cyr, A.R., Woodfield, G.W., De Andrade, J.P., Spanheimer, P.M., Li, T., Sugg, S.L., Lal, G., Domann, F.E., et al. (2015). The role of Tcfap2c in tumorigenesis and cancer growth in an activated Neu model of mammary carcinogenesis. Oncogene *34*, 6105–6114.

Pawlak, M., and Jaenisch, R. (2011). De novo DNA methylation by Dnmt3a and Dnmt3b is dispensable for nuclear reprogramming of somatic cells to a pluripotent state. Genes Dev. *25*, 1035–1040.

Polo, J.M., Anderssen, E., Walsh, R.M., Schwarz, B.A., Nefzger, C.M., Lim, S.M., Borkent, M., Apostolou, E., Alaei, S., Cloutier, J., et al. (2012). A molecular roadmap of reprogramming somatic cells into iPS cells. Cell *151*, 1617–1632.

Robinson, M.D., McCarthy, D.J., and Smyth, G.K. (2010). edgeR: a Bioconductor package for differential expression analysis of digital gene expression data. Bioinformatics *26*, 139–140.

Schemmer, J., Araúzo-Bravo, M.J., Haas, N., Schäfer, S., Weber, S.N., Becker, A., Eckert, D., Zimmer, A., Nettersheim, D., and Schorle, H. (2013). Transcription factor TFAP2C regulates major programs required for murine fetal germ cell maintenance and haploinsufficiency predisposes to teratomas in male mice. PLoS ONE *8*, e71113.

Shakiba, N., White, C.A., Lipsitz, Y.Y., Yachie-Kinoshita, A., Tonge, P.D., Hussein, S.M., Puri, M.C., Elbaz, J., Morrissey-Scoot, J., Li, M., et al. (2015). CD24 tracks divergent pluripotent states in mouse and human cells. Nat. Commun. *6*, 7329.

Shen, Y., Yue, F., McCleary, D.F., Ye, Z., Edsall, L., Kuan, S., Wagner, U., Dixon, J., Lee, L., Lobanenkov, V.V., and Ren, B. (2012). A map of the cis-regulatory sequences in the mouse genome. Nature *488*, 116–120.

Sommer, C.A., Stadtfeld, M., Murphy, G.J., Hochedlinger, K., Kotton, D.N., and Mostoslavsky, G. (2009). Induced pluripotent stem cell generation using a single lentiviral stem cell cassette. Stem Cells *27*, 543–549.

Soufi, A., Donahue, G., and Zaret, K.S. (2012). Facilitators and impediments of the pluripotency reprogramming factors' initial engagement with the genome. Cell *151*, 994–1004.

Stadtfeld, M., Maherali, N., Borkent, M., and Hochedlinger, K. (2010). A reprogrammable mouse strain from gene-targeted embryonic stem cells. Nat. Methods *7*, 53–55.

Stadtfeld, M., Maherali, N., Breault, D.T., and Hochedlinger, K. (2008). Defining molecular cornerstones during fibroblast to iPS cell reprogramming in mouse. Cell Stem Cell *2*, 230–240.

Takahashi, K., and Yamanaka, S. (2006). Induction of pluripotent stem cells from mouse embryonic and adult fibroblast cultures by defined factors. Cell *126*, 663–676.

Takahashi, K., and Yamanaka, S. (2016). A decade of transcription factor-mediated reprogramming to pluripotency. Nat. Rev. Mol. Cell Biol. *17*, 183–193.

Vidal, S.E., Amlani, B., Chen, T., Tsirigos, A., and Stadtfeld, M. (2014). Combinatorial modulation of signaling pathways reveals cell-type-specific requirements for highly efficient and synchronous iPSC reprogramming. Stem Cell Reports *3*, 574–584.

Xi, Y., and Li, W. (2009). BSMAP: whole genome bisulfite sequence MAPping program. BMC Bioinformatics *10*, 232.

STAR★METHODS

KEY RESOURCES TABLE

REAGENT or RESOURCE	SOURCE	IDENTIFIER
Antibodies		
Rat monoclonal anti-Mouse Thy1.2 eFluor 450	Thermo Fisher Scientific	Cat#48-0902-82; RRID: AB_1272200; 53-2.1
Mouse monoclonal anti-Human/Mouse SSEA-1 eFluor 660	Thermo Fisher Scientific	Cat#50-8813-42; RRID: AB_11219681; MC-480
Rat monoclonal anti-Mouse PDGFRβ PE	Thermo Fisher Scientific	Cat#12-1402-81; RRID: AB_529484; APB5
Rat monoclonal anti-Mouse VCAM1 PE	Thermo Fisher Scientific	Cat#12-1061-82; RRID: AB_2572573; 429
Rat monoclonal anti-Human/Mouse CD44 PE	Thermo Fisher Scientific	Cat#12-0441-82; RRID: AB_465664; IM7
Rat monoclonal anti-Mouse CD73 PE	Thermo Fisher Scientific	Cat#12-0731-82; RRID: AB_763513; eBioTY/11.8
Rat monoclonal anti-Mouse CD49d PE	Thermo Fisher Scientific	Cat#12-0492-82; RRID: AB_465697; R1-2
Rat monoclonal anti-Mouse Sca-1 PE-Cy7	Thermo Fisher Scientific	Cat#25-5981-82; RRID: AB_469669; D7
Rat monoclonal anti-Mouse CD71 PE	Thermo Fisher Scientific	Cat#12-0711-82; RRID: AB_465740; R17217
Rat monoclonal anti-Mouse EpCAM PE	Thermo Fisher Scientific	Cat#12-5791-82; RRID: AB_953615; G8.8
Rat monoclonal anti-Mouse ICAM1 PE	Thermo Fisher Scientific	Cat#12-0542-82; RRID: AB_529540; eBioKAT-1
Rat monoclonal anti-Mouse CD24 PE	Thermo Fisher Scientific	Cat#12-0242-82; RRID: AB_465602; M1/69
Rat monoclonal anti-Mouse Prom1 PE	Thermo Fisher Scientific	Cat#12-1331-82; RRID: AB_465849; 13A4
Rat monoclonal anti-Mouse Podxl PE	R&D Systems	Cat#FAB1556P; 192703
Mouse monoclonal anti-Mouse CEACAM1 PE	Thermo Fisher Scientific	Cat#12-0661-80; RRID: AB_1311201; CC1
Rat monoclonal anti-Human/Mouse E-Cadherin PE	BioLegend	Cat#147303; RRID: AB_2563039; DECMA-1
Rat monoclonal anti-Mouse c-Kit PE	Thermo Fisher Scientific	Cat#12-1171-82; RRID: AB_465813; 2B8
Rat monoclonal anti-Mouse PECAM1 PE	Thermo Fisher Scientific	Cat#12-0311-82; RRID: AB_465632; 390
Rat monoclonal isotype control PE	Thermo Fisher Scientific	Cat#12-4321-41; RRID: AB_1518774; eBR2a
Chemicals, Peptides, and Recombinant Proteins		
Doxycycline	Sigma Aldrich	Cat#D9891-100G
L-Ascorbic Acid	Sigma Aldrich	Cat#A92902
Puromycin	Thermo Fisher Scientific	Cat#A1113802
CHIR-99021	Tocris	Cat#4423
TGFβ RI Kinase Inhibitor II	Millipore	Cat#616452
Lipofectamine 2000	Thermo Fisher Scientific	Cat#11668027
TransIT-293 Transfection Reagent	Mirus	Cat#MIR-2700
Polybrene	Sigma Aldrich	Cat#TR-1003-G

(*Continued on next page*)

Continued

REAGENT or RESOURCE	SOURCE	IDENTIFIER
Critical Commercial Assays		
Vector Red Alkaline Phosphatase Substrate Kit	Vector Laboratories	Cat#SK-5100
RNeasy Micro Kit	Qiagen	Cat#74004
High-Capacity RNA-to-cDNA kit	Thermo Fisher Scientific	Cat#4387406
Brilliant III SYBR Master Mix	Agilent	Cat#600882
NEBNext Ultra Directional RNA Library Prep Kit	New England BioLabs	Cat#E7420S
Nextera DNA Library Preparation Kit	Illumina	Cat#FC-121-1030
MinElute Reaction Cleanup Kit	Qiagen	Cat#28204
Deposited Data		
RNA-seq	This study	GEO: GSE106835
RNA-seq	This study	GEO: GSE106836
ATAC-seq	This study	GEO: GSE106834
WGBS	This study	GEO: GSE106525
Experimental Models: Cell Lines		
Mouse embryonic fibroblasts from B6;129S4-Gt(ROSA) 26Sor$^{tm1(rtTA*M2)Jae}$ Col1a1$^{tm1(tetO-Pou5f1,-Klf4,-Sox2,-Myc)Hoch}$ Pou5f1^{tm2Jae}/J	This study	N/A
Tail tip fibroblasts from B6;129S4-*Gt(ROSA)26Sor*$^{tm1(rtTA*M2)Jae}$ *Col1a1*$^{tm1(tetO-Pou5f1,-Klf4,-Sox2,-Myc)Hoch}$ *Pou5f1*^{tm2Jae}/J	This study	N/A
Mouse embryonic fibroblasts from B6;129S4-*Gt(ROSA) 26Sor*$^{tm1(rtTA*M2)Jae}$*Col1a1*$^{tm1(tetO-Pou5f1,-Klf4,-Sox2,-Myc)Hoch}$ *Col1a1*$^{tm1(tetO-Pou5f1,-Klf4,-Sox2,-mCherry)}$*Pou5f1*^{tm2Jae}/J	This study	N/A
Mouse embryonic fibroblasts from *Gt(ROSA)26Sor*$^{tm1(rtTA*M2)Jae}$ *Col1a1*$^{tm3(tetO-Pou5f1,-Sox2,-Klf4,-Myc)Jae}$Pou5f1^{tm2Jae}/J	This study	N/A
Mouse embryonic fibroblasts from B6;129S-*Gt(ROSA) 26Sor*$^{tm1(rtTA*M2)Jae}$*Sox2*^{tm2Hoch}/J	This study	N/A
Mouse embryonic fibroblasts from *Tfap2c*$^{fl/fl}$	This study	N/A
Mouse embryonic fibroblasts from *Bex2*^{EGFP}	This study	N/A
Experimental Models: Organisms/Strains		
Mouse: B6.Cg-Gt(ROSA)26Sor$^{tm1(rtTA*M2)Jae}$/J	The Jackson Laboratory	Cat#006965
Mouse: B6;129S4-Col1a1$^{tm1(tetO-Pou5f1,-Klf4,-Sox2,-Myc)Hoch}$ Pou5f1^{tm2Jae}/J	The Jackson Laboratory	Cat#011001
Mouse: B6;129S4-Gt(ROSA)26Sor$^{tm1(rtTA*M2)Jae}$ Col1a1$^{tm1(tetO-Pou5f1,-Klf4,-Sox2,-mCherry)}$	Bar-Nur et al., 2014	N/A
Mouse: *Gt(ROSA)26Sor*$^{tm1(rtTA*M2)Jae}$ *Col1a1*$^{tm3(tetO-Pou5f1,-Sox2,-Klf4,-Myc)Jae}$/J	The Jackson Laboratory	Cat#011004
Mouse: B6;129S4-*Pou5f1*^{tm2Jae}/J	The Jackson Laboratory	Cat#008214
Mouse: B6;129S-*Sox2*^{tm2Hoch}/J	The Jackson Laboratory	Cat#017592
Mouse: *Tfap2c*$^{fl/fl}$	Schemmer et al., 2013	N/A
Mouse: *Bex2*^{EGFP}	Ito et al., 2014	N/A
Oligonucleotides		
Oct4 KiCqStart SYBR Green Primers	Sigma Aldrich	Cat#KSPQ12012 M_Pou5f1_2
Klf4 KiCqStart SYBR Green Primers	Sigma Aldrich	Cat#KSPQ12012 M_Klf4_1
Hprt KiCqStart SYBR Green Primers	Sigma Aldrich	Cat#KSPQ12012 M_Hprt_1
Utf1 sgRNA: 5′-GACTGATAACAAAGCTTTAT-3′	This study	N/A
Recombinant DNA		
pHAGE-Tet-STEMCCA	Sommer et al., 2009	N/A
FUdeltaGW-rtTA	Addgene	Cat#19780
pLV-TetO-Oct4	Addgene	Cat#19766
pLV-tetO-Sox2	Addgene	Cat#19765

(*Continued on next page*)

Continued

REAGENT or RESOURCE	SOURCE	IDENTIFIER
pLV-tetO-Klf4	Addgene	Cat#19764
pLV-tetO-Myc	Addgene	Cat#19763
pLV-TetO-Tfap2c	Addgene	Cat#70269
pLV-Bex2	VectorBuilder	Cat#VB171031-1148juj
pHAGE2-Cre-IRES-PuroR	Addgene	Cat#30205
Lenti-entry-puro	Addgene	Cat#85745
Software and Algorithms		
FlowJo	FlowJo, LLC	https://www.flowjo.com/
Integrative Genomics Viewer	Broad Institute	http://software.broadinstitute.org/software/igv/
STAR	Dobin et al., 2013	https://github.com/alexdobin/STAR/releases
HTSeq	Anders et al., 2015	https://htseq.readthedocs.io/en/release_0.10.0/
EdgeR	Robinson et al., 2010	https://doi.org/10.18129/B9.bioc.edgeR
BWA	Li and Durbin, 2009	http://bio-bwa.sourceforge.net
Hotspot	John et al., 2011	https://github.com/StamLab/hotspot/releases/tag/v4.1.1
BSMap	Xi and Li, 2009	https://code.google.com/archive/p/bsmap/

CONTACT FOR REAGENT AND RESOURCE SHARING

Further information and requests for resources and reagents should be directed to and will be fulfilled by the Lead Contact, Konrad Hochedlinger (hochedlinger@molbio.mgh.harvard.edu).

EXPERIMENTAL MODEL AND SUBJECT DETAILS

Animal Care

All mice used in the study were housed and bred in the Center for Comparative Medicine at Massachusetts General Hospital AAALAC-accredited mouse facility in Specific Pathogen Free (SPF) rooms. All procedures involving mice adhered to the guidelines of the approved Massachusetts General Hospital Institutional Animal Care and Use Committee (IACUC) protocol #2006N000104.

Fibroblast Derivation

Col1a1-tetO-OKSM^{homo} *Oct4-GFP*^{homo} mice were mated with either *R26-rtTA*^{homo} or *Col1a1-tetO-OKSmCherry*^{homo} *R26-rtTA*^{homo} mice to generate *Col1a1-tetO-OKSM*^{het} *R26-rtTA*^{het} *Oct4-GFP*^{het} (het/het) or *Col1a1-tetO-OKSM/OKSmCherry R26-rtTA*^{het} *Oct4-GFP*^{het} (3/4) embryos, respectively. Het/het mice were mated to each other to generate *Col1a1-tetO-OKSM*^{homo} *R26-rtTA*^{homo} and *Col1a1-tetO-OKSM*^{het} *R26-rtTA*^{homo} embryos. *Col1a1-tetO-OSKM*(Jae)^{homo} *R26-rtTA*^{homo} mice (Carey et al., 2011) were mated with *Oct4-GFP*^{homo} mice to generate *Col1a1-tetO-OSKM*(Jae)^{het} *R26-rtTA*^{het} *Oct4-GFP*^{het} embryos. DR4 mice were bred with BALB/c to generate DR4 embryos. *Sox2-GFP* mice were mated with *R26-rtTA* mice to generate *R26-rtTA*^{het} *Sox2-GFP*^{het} embryos. *Bex2-GFP*^{het} (a *Bex2* KO reporter allele) females were mated with wild-type males to generate *Bex2*$^{GFP/Y}$ and littermate wild-type control embryos (Ito et al., 2014). *Tfap2c*$^{fl/fl}$ embryos were also generated (Schemmer et al., 2013). Embryos were harvested at E13.5-15.5, the head and internal organs were removed, and the remaining tissue was chopped and dissociated with trypsin to isolate MEFs. Tail tips of neonatal het/het mice were chopping and dissociating with trypsin to isolate TTFs.

METHOD DETAILS

Cell Culture and Reprogramming

MEFs were maintained in MEF medium [DMEM (Invitrogen) supplemented with L-glutamine, penicillin/streptomycin, nonessential amino acids, β-mercaptoethanol, and 10% FBS (Invitrogen)] and expanded to p3 or p4 prior to reprogramming. TTFs were expanded in MEF medium to p1 prior to reprogramming. DR4 MEFs were expanded to p3 or p4 and then irradiated (3,000 rads) to generate feeders. Fibroblasts were reprogrammed at low density on gelatin-coated cell culture plates, whereas sorted cells were plated on gelatin with irradiated DR4 feeder MEFs. Reprogramming experiments were performed in ESC medium [KO-DMEM (Invitrogen)

with L-glutamine, penicillin/streptomycin, nonessential amino acids, β-mercaptoethanol, 1,000 U/mL LIF, and 15% FBS (Invitrogen)] supplemented with 1 ug/mL of doxycycline (dox) and 50 ug/mL of ascorbic acid (AA), unless indicated otherwise. For specific experiments, 3 uM GSKi (CHIR-99021, Tocris) or 1 uM Alk5i (EMD-616452, Calbiochem) were added to the ESC medium. Reprogramming intermediates derived from het/het MEF were used for the characterization of surface marker expression and the corresponding RNA-seq analysis. All adjusted reprogramming efficiency assays, RNA-seq of Eff and Ineff cells, ATAC-seq, and WGBS were done using reprogramming intermediates derived from 3/4 MEFs. Established 3/4 iPSCs were cultured in ESC medium and analyzed at p10 for molecular studies.

Flow Cytometry and Cell Sorting

MEFs, reprogramming intermediates, or iPSCs were dissociated with trypsin. For analysis of trypsin sensitive antigens (CD44, E-cadherin, and PECAM1) EDTA was used instead. Cells were then stained with combinations of the following antibodies: anti-mouse Thy1.2 (53-2.1), SSEA-1 (MC-480), PDGFRβ (APB5), VCAM1 (429), CD44 (IM7), CD73 (eBioTY/11.8), CD49d (R1-2), Sca-1 (D7), CD71 (R17217), EpCAM (G8.8), ICAM1 (eBioKAT-1), CD24 (M1/69), Prom1 (13A4), Podxl (FAB1556P), CEACAM1 (CC1), E-Cadherin (DECMA-1), c-Kit (2B8), PECAM1 (390), or an isotype control (eBR2a), all directly conjugated to phycoerythrin (PE), PE-Cy7, eFluor 450, or eFluor 660. DAPI was used for dead cell exclusion. For molecular analyses, 3/4 iPSCs were sorted for *Oct4*-GFP, to eliminate contamination with differentiating cells. Flow cytometry was performed on a LSR-II (BD) and cell sorting was performed on a FACSAria-II (BD). Analysis was done with FlowJo software.

Assay for Adjusted Reprogramming Efficiency

To determine reprogramming efficiency, 10,000 sorted cells were plated in individual wells of 6-well dishes and exposed to dox for 0, 3, 6, 9, or 12 additional days. Dox was then withdrawn for at least 3 days prior to alkaline phosphatase (AP) staining (Vector Laboratories). AP^+ dox-independent iPSCs were counted manually. Reprogramming efficiency was calculated as the number of iPSC colonies divided by the number of cells plated. To determine plating efficiency, cells from the same sort were sorted directly into 96-well plates with 24 wells each of 5 cells, 10 cells, 20 cells, and 40 cells. These wells were then exposed to dox for 4 additional weeks. Each well was assessed for *Oct4*-GFP^+ colonies by inverted fluorescent microscopy. Cells were then dissociated with trypsin and plates were analyzed by flow cytometry on a MACSQuant (Miltenyi). Each well was scored individually as *Oct4*-GFP^+, $mCherry^+$, or negative for both fluorescent markers. A limiting dilution analysis was used to determine plating efficiency. Briefly, the log of % negative wells was determined for each input cell number and plotted to determine a best-fit line. Based on a Poisson distribution, the number of cells required for 37% of wells to be negative is the limiting dilution (LD). Plating efficiency was calculated as the inverse of the LD. Adjusted reprogramming efficiency was determined by dividing the reprogramming efficiency by the plating efficiency.

qRT-PCR

RNA purified from cells using the RNeasy Micro Kit (QIAGEN) was converted to cDNA using the High-Capacity RNA-to-cDNA kit (Applied Biosystems). qRT-PCR reactions were set up in triplicate using the Brilliant III SYBR Master Mix (Agilent Genomics) and KiCqStart SYBR Green Primers (Sigma-Aldrich) to *Oct4* (M_Pou5f1_2), *Klf4* (M_Klf4_1), and *Hprt* (M_Hprt_1). Reactions were run on the LightCycler 480 PCR machine (Roche) with 40 cycles of 30 s at 95C, 30 s at 60C and 30 s at 72C.

RNA-seq

Three replicates each of het/het MEFs, d3 SSEA-1^-, d3 SSEA-1^+, d6 SSEA-1^-, d6 SSEA-1^+, d9 SSEA-1^-, d9 SSEA-1^+, d12 SSEA-1^-, d12 SSEA-1^+, SSEA-1^- after 12d of dox followed by at least 3d of withdrawal, and iPS (SSEA-1^+ cells after 12d of dox followed by at least 3d of withdrawal) were isolated by FACS. Additionally, 2 replicates each of 3/4 MEFs, d3 Ineff, d3 Eff, d6 Ineff, d6 Eff, and *Oct4*-GFP^+ iPSCs were isolated by FACS. RNA was extracted from sorted cells using the RNeasy Micro Kit (QIAGEN). cDNA libraries were generated using the NEBNext Ultra Directional RNA Library Prep Kit (NEB) based on poly-A selection. RNA and libraries were validated using a bioanalyzer (Agilent). Sequencing (50 cycles, paired-end) was performed using the HiSeq 2500 platform (Illumina), resulting in ~30 million reads per sample.

ATAC-seq

Two replicates each of 3/4 MEFs, d3 Ineff, d3 Eff, d6 Ineff, d6 Eff, and *Oct4*-GFP^+ iPSCs were isolated by FACS. ATAC-seq libraries were generated as previously described (Buenrostro et al., 2013). Briefly, 50,000 sorted cells were resuspended in nuclear isolation buffer (10 mM Tris-HCl pH 7.4, 10 mM NaCl, 3 mM MgCl2, 0.1% IGEPAL). Nuclei were then treated with Tn5 transposase (Illumina). DNA was isolate using the MinElute Kit (QIAGEN) and PCR-amplified using barcoded Nextera primers (Illumina). The DNA libraries were validated using a bioanalyzer (Agilent). Sequencing (50 cycles, paired-end) was performed using the HiSeq 2500 platform (Illumina), resulting in ~45 million reads per sample.

Whole Genome Bisulfite Sequencing (WGBS)

3/4 MEFs, d3 Ineff, d3 Eff, d6 Ineff, d6 Eff, and *Oct4*-GFP^+ iPSCs were isolated by FACS. Genomic DNA was purified from sorted cells, and WGBS library construction was performed as previously described (Gifford et al., 2013). Genomic fragments were sequenced using the HiSeq 2500 platform (Illumina).

siRNA Transfection and Analysis

Cells were transfected using Lipofectamine 2000 (Thermo Fisher) with pooled siRNA at a final concentration of 15-20 nM. All siRNA pools were esiRNA (Sigma-Aldrich) except for the siRNA targeting *Dmrtc2* (GE-Dharmacon). Cells were treated with siRNA at d0, d3, d6, and d9 of reprogramming, after which dox was withdrawn. After 3-5 additional days, dox-independent iPSCs were stained for AP and reprogramming efficiency was determined (see above). Alternatively, d3 and d6 intermediates were analyzed by flow cytometry.

Lentivirus Production and Infections

293T cells were transfected with plasmids for lentiviral (LV) packaging (*VSV-G* and *Δ8.9*) and LV plasmids for either *Stemcca*, *rtTA*, *tetO-Oct4*, *tetO-Sox2*, *tetO-Klf4*, *tetO-Myc*, *Bex2*, *tetO-Tfap2c*, *Cre-IRES-Puromycin*, or *Puromycin*, using TransIT-293 Transfection Reagent (Mirus) to generate individual lentiviruses. MEFs were infected with virus combinations using Polybrene (Sigma). *R26-rtTA*^{het} *Sox2-GFP*^{het} MEFs were treated with LV-*Oct4*, LV-*Sox2*, LV-*Klf4*, and LV-*Myc* for individual vector reprogramming. *Bex2*$^{GFP/Y}$ and littermate control MEFs were infected with LV-*Stemcca* and LV-*rtTA*. *Tfap2c*$^{flox/flox}$ MEFs were infected with LV-*Stemcca*, LV-*rtTA*, and either LV-*Cre-IRES-Puro* or a LV-*Puro* control followed by puromycin selection prior to reprogramming. Het/het MEFs were infected with either LV-*Bex2*, LV-*Tfap2c*, or a LV-*Puro* control.

Generation of *Utf1* Reporter Cells

Utf1-GFP reporter ESC lines were generated through CRISPR/Cas mediated gene targeting. A targeting construct was designed to integrate an E2A-GFP cassette in-frame with the final exon of *Utf1.* The construct was generated via PCR amplification and Gibson assembly (New England Biolabs) of E2A-GFP flanked on either side by 500bp of homology to the *Utf1* locus. The targeting construct was cotransfected using Lipofectamine 2000 (Thermo) with a *Utf1*-targeting sgRNA (5′-GACTGATAACAAAGCTTTAT-3′) and a *Cas9* expression construct into V6.5 ESCs that had previously been targeted with doxycycline inducible *Col1a1-OKSM* and *Rosa26-rtTA*. One week following the transfection, GFP+ cells were isolated by FACS and clonally expanded for analysis by Southern blot. Positive clones were injected into blastocysts and the resultant embryos were harvested at E15.5 for the preparation of high-grade chimeric MEFs.

QUANTIFICATION AND STATISTICAL ANALYSIS

Statistical Analysis

Statistics including the number of replicates, mean, and SD are reported in the Figures and the Figure Legends. Data is judged to be statistically significant by two-tailed Student's t test ($p < 0.05$), where appropriate.

RNA-seq

RNA-seq reads were aligned to the mouse (mm9) reference transcriptome using STAR, a splice-aware alignment program. Read counts over transcripts were calculated using HTSeq based on a current Ensembl annotation file for NCBI37/mm9 assembly. For differential expression analysis the EdgeR package was used. DEGs were determined by a 2-fold or greater difference between two samples and a false discovery rate (FDR) below 0.05.

ATAC-seq

ATAC-seq reads were aligned to the mouse (mm9) reference genome using the BWA package. Only fragments with both ends unambiguously mapped to the genome that were longer than 100 bp were used for further analysis. Hotspot was used to detect significant peaks with an FDR cutoff of 0.05. Since the detected peaks were highly consistent between individual biological replicates, we merged replicate peak sets to produce the sets representing each population (MEF, d3 Ineff, d3 Eff, d6 Ineff, d6 Eff, and iPSC). The resulting peak regions were analyzed for changes in read density between populations. For the analysis of overlap between peak regions, we used the cutoff of 30% overlap in at least one of the two compared regions. DARs were determined by RPKM values for peak regions differing by 2-fold or greater between samples and an FDR below 0.05. TF-binding motif analysis was done with AME (http://meme-suite.org/tools/ame).

WGBS

Reads were aligned to the mouse (mm9) reference genome using BSMap. Methylation levels of individual CpGs were determined by observing bisulfite conversion in the aligned read compared to the reference genome. Region methylation levels were computed using CpGs covered by at least 5x in at least 4 samples. Differential methylation analysis was performed by using Fisher's exact test to measure the significance of differential methylation at each CpG in a region. P values of CpGs in a region were combined using Fisher's method to calculate a region p value. Regions covered by at least 3 CpGs, with a p value of less than 0.01, and showing a weighted methylation difference of at least 30% were called differentially methylated.

DATA AND SOFTWARE AVAILABILITY

The accession number for the sequencing data reported in this paper is GEO: GSE106838.